~67% cell viability levels, respectively, although cross-linked $A\beta_{42}$ (non-significantly) towards modestly higher toxicity. Retinoic acid treatment increased cell viability ~94% higher than untreated cross-linked $A\beta_{42}$ as well as un-cross-linked $A\beta_{42}$ ($p < 0.01$) (Fig. 3).

Thus, retinoic acid was highly effective inhibitors of low-n $A\beta_{42}$ oligomer-induced cellular toxicity.

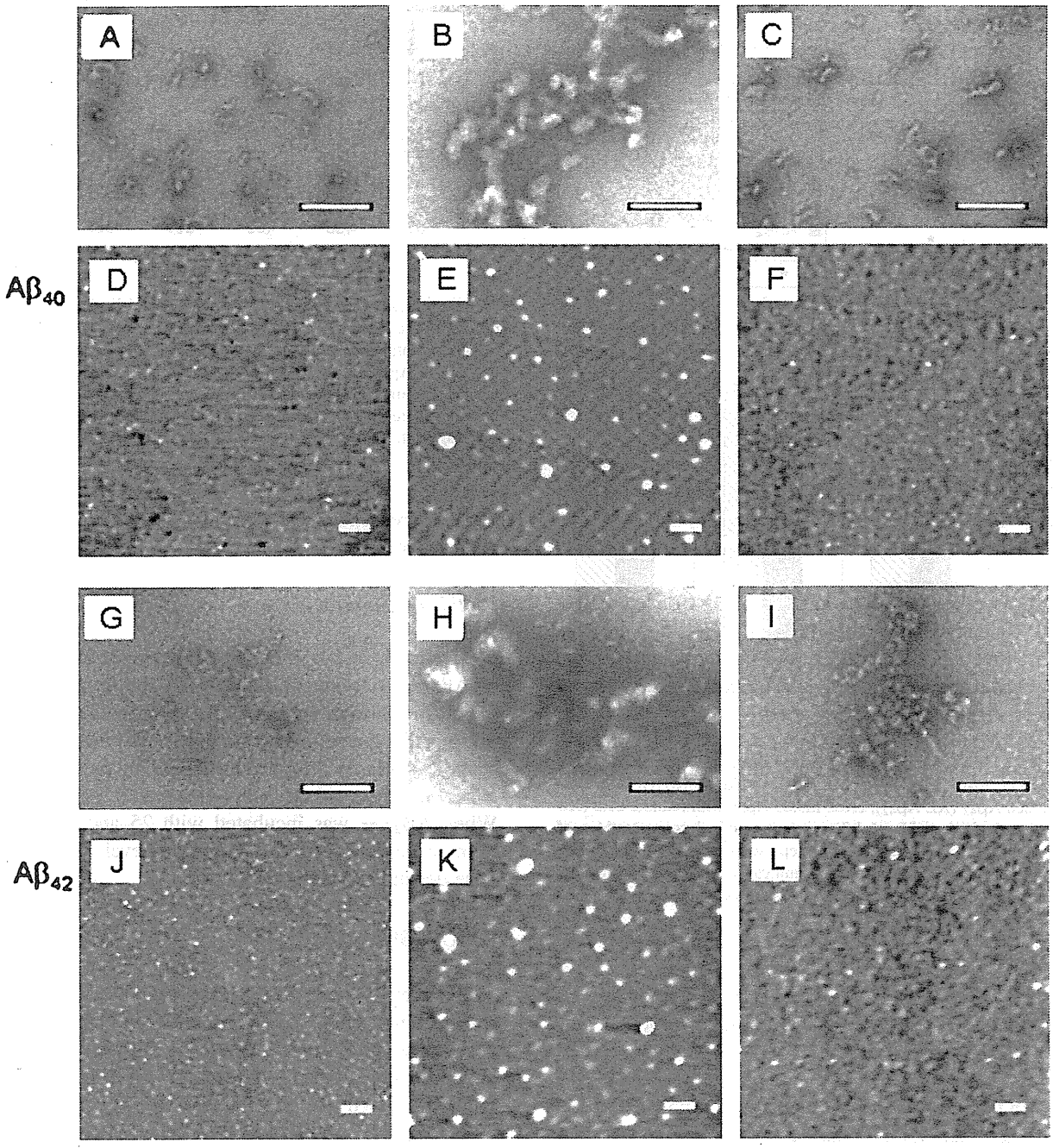

Fig. 2. Morphological analysis of $A\beta_{40}$ (A, B, and C) or $A\beta_{42}$ (G, H, and I) assemblies by EM. Un-cross-linked Aβ alone (A and G), cross-linked Aβ alone (B and H), and Aβ cross-linked with 250 μM retinoic acid (C and I) were examined by EM. Morphological analysis of $A\beta_{40}$ (D, E, and F) or $A\beta_{42}$ (J, K, and L) assemblies by AFM. Un-cross-linked Aβ alone (D and J), cross-linked Aβ alone (E and K), and Aβ cross-linked with 250 μM retinoic acid (F and L) were examined by AFM (Scale bars: 100 nm.).

Table 1
Morphological analysis of Aβ assemblies

Assembly	Diameter[a]	Height[b]
Uncross-linked $A\beta_{40}$	1.43 ± 0.16 (63)	0.20 ± 0.03 (31)
Cross-linked $A\beta_{40}$	10.69 ± 1.87 (42)	0.88 ± 0.17 (30)
Cross-linked $A\beta_{40}$ with retinoic acid	1.51 ± 0.15 (50)	0.34 ± 0.05 (38)
Uncross-linked $A\beta_{42}$	2.15 ± 0.20 (57)	0.31 ± 0.09 (46)
Cross-linked $A\beta_{42}$	21.22 ± 3.50 (32)	1.09 ± 0.56 (49)
Cross-linked $A\beta_{42}$ with retinoic acid	2.18 ± 0.19 (56)	0.36 ± 0.10 (38)

[a]Mean diameter ± SE, in nm, is listed for (n) Aβ assemblies visualized by EM. [b]Mean height ± SE, in nm, is listed for (n) Aβ assemblies visualized by AFM.

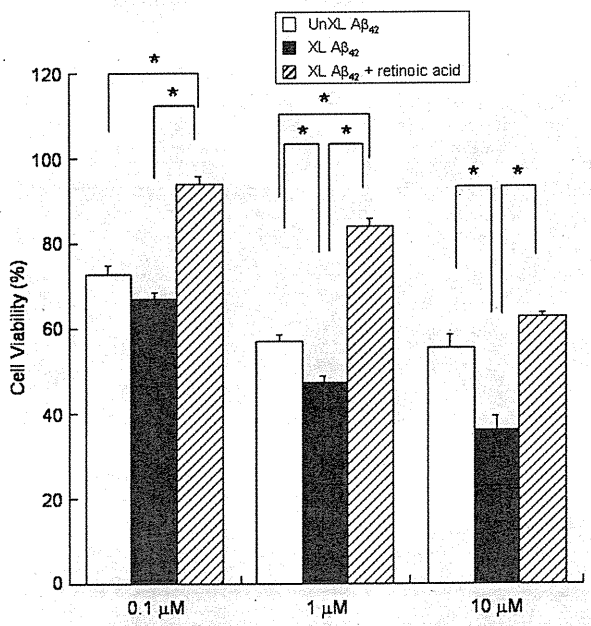

Fig. 3. Cell viability. MTT assays were performed on HEK293 cells incubated 22 h with un-cross-linked $A\beta_{42}$ (UnXL $A\beta_{42}$), cross-linked $A\beta_{42}$ (XL $A\beta_{42}$), cross-linked $A\beta_{42}$ with retinoic acid (XL $A\beta_{42}$ + retinoic acid) of $A\beta_{42}$ at final nominal concentrations of 0.1, 1, and 10 μM. Each column represents means ± S.E. ($n = 12$). Differences reaching statistical significance are noted by line segments between samples, along with their associated *p-values*, where * signifies $p < 0.01$.

Characterization of the fluorescence emission of retinoic acid in the presence or absence of Aβ fragments

In the absence of Aβ fragments, retinoic acid gave a maximum fluorescence emission at 600 nm with an excitation at 485 nm (Fig. 4). In the presence of $A\beta_{25\text{-}35}$, retinoic acid gave a restrained fluorescence emission at 600 nm with an excitation maximum at 485 nm (Fig. 4). On the other hand, a minimal change

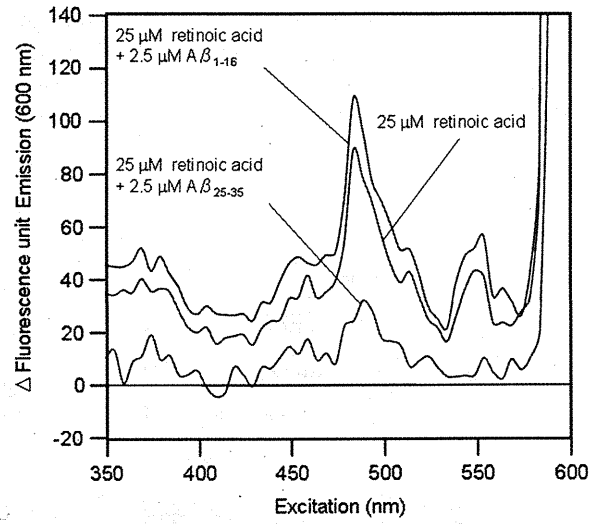

Fig. 4. Fluorescence emission of retinoic acid monitored at emission 600 nm in the presence or absence of Aβ fragments. The reaction mixtures containing 25 μM retinoic acid, 0–2.5 μM Aβ fragment [$A\beta_{1\text{-}16}$ or $A\beta_{25\text{-}35}$], and 10 mM phosphate buffer, pH 7.4, were measured immediately at emission 600 nm at 25°C. The fluorescence of only Aβ fragment was subtracted from that of retinoic acid with Aβ fragment. These are representative patterns of 3 independent experiments.

in the fluorescence spectra was observed when retinoic acid was mixed with $A\beta_{1\text{-}16}$ (Fig. 4).

Peptide aggregation assay

As shown in Fig. 5A and B, when fresh $A\beta_{1\text{-}16}$ or $A\beta_{25\text{-}35}$ was incubated at 37°C, the fluorescence of ThT followed a characteristic sigmoidal curve. When $A\beta_{1\text{-}16}$ was incubated with 25 and 250 μM retinoic acid, no significant change in the fluorescence was observed throughout the reaction (Fig. 5A). When $A\beta_{25\text{-}35}$ was incubated with 25 and 250 μM retinoic acid, the final equilibrium level decreased dose-dependently (Fig. 5B).

DISCUSSION

We previously reported that vitamin A and β-carotene not only inhibit Aβ fibrillation but also destabilize preformed Aβ fibrils [13]. The anti-amyloidogenic and fibril-destabilizing activities of vitamin A and β-carotene were in the order of retinol = retinal > β-carotene > retinoic acid [13]. Here we showed that vitamin A and β-carotene dose-dependently inhibit oligomerization of $A\beta_{40}$ and $A\beta_{42}$. Antioligomeric activities of vitamin A and β-carotene for $A\beta_{42}$ were higher than those for $A\beta_{40}$.

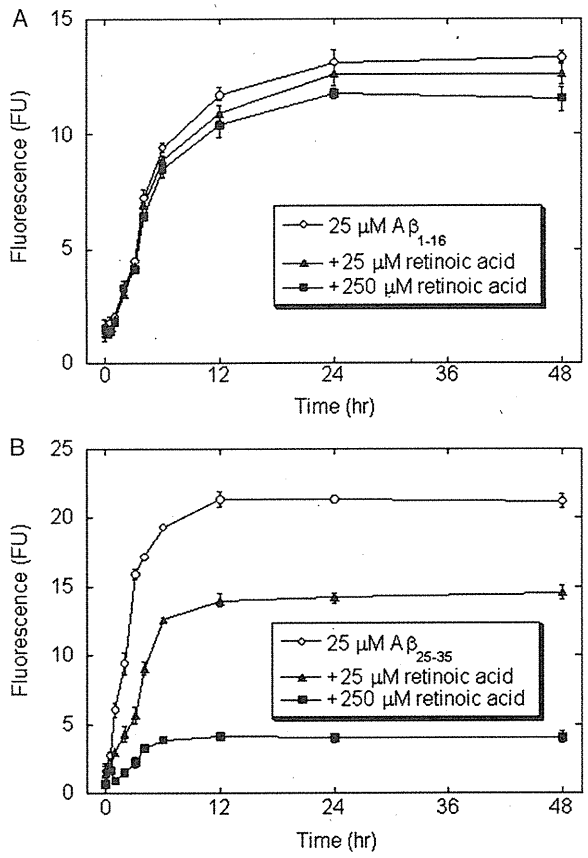

Fig. 5. Effects of retinoic acid on the kinetics of $A\beta_{1-16}$ (A) and $A\beta_{25-35}$ (B) aggregation from fresh $A\beta_{1-16}$ and $A\beta_{25-35}$, respectively. The reaction mixtures containing 25 μM $A\beta_{1-16}$ (A) or 25 μM $A\beta_{25-35}$ (B), 10 mM phosphate buffer, pH 7.4, and 0 (○), 25 (□), or 250 μM (■) of retinoic acid, were incubated at 37°C for the indicated times. Binding is expressed as mean fluorescence (in arbitrary fluorescence units (FU)) ± S.E. Each figure is a representative pattern of 3 independent experiments.

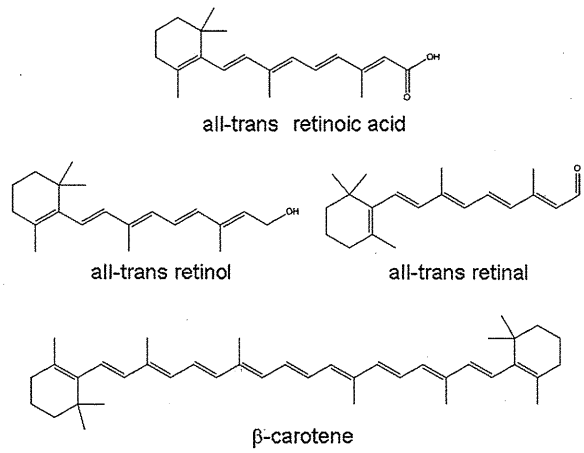

Fig. 6. Structures of all-trans retinol, all-trans retinal, all-trans retinoic acid, and β-carotene.

Their binding affinity to $A\beta_{42}$ may be higher than that to $A\beta_{40}$. Our previous experiments established that cross-linked oligomers of $A\beta_{40}$ and $A\beta_{42}$ are more toxic than un-cross-linked Aβ [10, 11]. Actually, we confirmed that retinoic acid decreased the cytotoxicity by inhibition of $A\beta_{42}$ oligomerization. Interestingly, cross-linked $A\beta_{42}$ with retinoic acid was less toxic than un-cross-linked $A\beta_{42}$. It might be due to stability of $A\beta_{42}$ assemblies by cross-linking [10].

Their antioligomeric activities were in the order of retinoic acid > retinol = retinal > β-carotene. Taken together with the results of the aforementioned antifibrillation and antioligomerization experiments, retinol and retinal are more effective in inhibiting fibrillation rather than oligomerization. On the other hand, retinoic acid is more effective in inhibiting oligomerization rather than fibrillation. The hydroxyl group of retinol is successively converted into an aldehyde group (retinal) and a carboxyl group (retinoic acid). Some interesting structure–activity relationships could be considered. First, retinol, retinal, and β-carotene have no charge under physiological aqueous conditions, while retinoic acid is negatively charged because of the terminal carboxyl group (Fig. 6). Second, water solubility of retinoic acid, retinol, and retinal is in the order of retinoic acid > retinal > retinol under physiological conditions [20]. The negative charge and increased hydrophilicity might increase the binding affinity of retinoic acid to low-order oligomers, resulting in its inhibitory effects on oligomerization of $A\beta_{40}$ and $A\beta_{42}$ *in vitro*. On the other hand, aldehyde and hydroxyl groups may increase the binding affinity to high-order aggregates, resulting in its inhibitory effects on fibrillation.

In this study, we further examined how vitamin A inhibits Aβ aggregation by using fluorescence spectroscopy and ThT assay with N- and C-terminal Aβ fragments, $A\beta_{1-16}$ and $A\beta_{25-35}$. We previously characterization of the novel fluorescence of polyphenol, myricetin emitted at 575 nm with an excitation maximum at 430 nm in the presence of $A\beta_{40}$ fibrils revealed the specific binding of myricetin to $A\beta_{40}$ fibrils [17].

Our result that a fluorescence peak emitted at 600 nm with an excitation maximum at 485 nm of retinoic acid was greatly restrained in the presence of $A\beta_{25-35}$ would indicate the specific binding of retinoic acid to $A\beta_{25-35}$. In the following aggregation studies with the Aβ fragments, we actually confirmed that retinoic acid inhibited aggregation of $A\beta_{25-35}$, but not of $A\beta_{1-16}$. Thus, we speculate that the binding site of retinoic acid

would be the C-terminal portion of Aβ. Further studies, such as nuclear magnetic resonance experiments, are essential to reveal the binding mechanism in detail.

Patients with AD were reported to have low serum and plasma concentrations of vitamin A and β-carotene and defective transport and function of retinoic acid in the brain [21–26]. Higher β-carotene plasma concentrations were associated with better memory performance in the elderly [27]. Deprivation of vitamin A led to Aβ deposition in the rat brain [28], while treatment with retinoic acid resulted in a decrease in Aβ deposition and tau phosphorylation in an AD mouse model [29]. These reports implicate vitamin A and β-carotene in AD pathogenesis.

Vitamin A is synthesized by the central nervous system (CNS) more than by any other organs, and plays important roles in the development of the CNS [30–32]. Vitamin A was reported to protect embryonic neurons from oxidative damage and apoptosis by inhibiting of glutathione depletion [33]. Vitamin A may protect neurons against oxidative stress, which may result from aging, energy deficiency, inflammation, or excessive production of Aβ [34]. Finally, we have reported that vitamin A inhibits Aβ oligomerization as well as Aβ fibrillation [13] *in vitro*. Moreover, cell culture experiments with HEK 293 cells indicated that Aβ aggregates treated by vitamin A are less toxic than intact Aβ fibrils or Aβ oligomers. Further studies by using a more appropriated cell-line (e.g., primary cortical neurons) are needed to test a more realistic potentiality of the therapeutic capabilities of vitamin A.

Human plasma concentrations of vitamin A and β-carotene are 1.27–2.99 μM and 0.13–1.53 μM, respectively [25]. Vitamin A and β-carotene readily cross the blood-brain barrier [35, 36]. EC_{50} of vitamin A and β-carotene for Aβ oligomerization in our experimental model may be higher than their physiological concentrations in the brain. However, vitamin A and β-carotene may exhibit antioligomerization activities *in vivo* when administered in high doses that persist for a long time.

Vitamin A and β-carotene may act as key molecules for the development of preventive and/or therapeutic approaches for AD.

ACKNOWLEDGMENTS

This work was supported by a grant for Knowledge Cluster Initiative [High-Tech Sensing and Knowledge Handling Technology (Brain Technology)] (M.Y.), Grant-in-Aid for Scientific Research (B) (20390242) (M.Y.), and Grant-in-Aid for Young Scientists (B) (K.O.) from the Ministry of Education, Culture, Sports, Science and Technology, Japan, grant to the Amyloidosis Research Committee from the Ministry of Health, Labour, and Welfare, Japan (M.Y. and K.O.), the Novartis Foundation for Gerontological Research (K.O.), and Alumni Association of the Department of Medicine at Showa University (K.O.).

Authors' disclosures available online (http://www.j-alz.com/disclosures/view.php?id=907).

REFERENCES

[1] Mattson MP (2004) Pathways towards and away from Alzheimer's disease. *Nature* **430**, 631-639.

[2] Hardy J, Selkoe DJ (2002) The amyloid hypothesis of Alzheimer's disease: Progress and problems on the road to therapeutics. *Science* **297**, 353-356.

[3] Kirkitadze MD, Bitan G, Teplow DB (2002) Paradigm shifts in Alzheimer's disease and other neurodegenerative disorders: The emerging role of oligomeric assemblies. *J Neurosci Res* **69**, 567-577.

[4] Walsh DM, Selkoe DJ (2007) Aβ oligomers - a decade of discovery. *J Neurochem* **101**, 1172-1184.

[5] Fancy DA, Kodadek T (1999) Chemistry for the analysis of protein-protein interactions: Rapid and efficient cross-linking triggered by long wavelength light. *Proc Natl Acad Sci U S A* **96**, 6020-6024.

[6] Bitan G (2006) Structural study of metastable amyloidogenic protein oligomers by photo-induced cross-linking of unmodified proteins. *Methods Enzymol* **413**, 217-236.

[7] Ono K, Condron MM, Ho L, Wang J, Zhao W, Pasinetti GM, Teplow DB (2008) Effects of grape seed-derived polyphenols on amyloid β-protein self-assembly and cytotoxicity. *J Biol Chem* **283**, 32176-32187.

[8] Wang J, Ono K, Dickstein DL, Arrieta-Cruz I, Zhao W, Qian X, Lamparello A, Subnani R, Ferruzzi M, Pavlides C, Ho L, Hof PR, Teplow DB, Pasinetti GM (2010) Carvedilol as a potential novel agent for the treatment of Alzheimer's disease. *Neurobiol Aging*, doi:10.1016/j.neurobiolaging.2010.05.004.

[9] Morinaga A, Ono K, Takasaki J, Ikeda T, Hirohata M, Yamada M (2011) Effects of sex hormones on Alzheimer's disease-associated β-amyloid oligomer formation *in vitro*. *Exp Neurol* **228**, 298-302.

[10] Ono K, Condron MM, Teplow DB (2009) Structure-neurotoxicity relationships of amyloid β-protein oligomers. *Proc Natl Acad Sci U S A* **106**, 14745-14750.

[11] Ono K, Condron MM, Teplow DB (2010) Effects of the English (H6R) and Tottori (D7N) familial Alzheimer disease mutations on amyloid β-protein assembly and toxicity. *J Biol Chem* **285**, 23186-23197.

[12] Ono K, Yamada M (2011) Low-n oligomers as therapeutic targets of Alzheimer's disease. *J Neurochem* **117**, 19-28.

[13] Ono K, Yoshiike Y, Takashima A, Hasegawa K, Naiki H, Yamada M (2004) Vitamin A exhibits potent antiamyloidogenic and fibril-destabilizing effects *in vitro*. *Exp Neurol* **189**, 380-392.

[14] Ono K, Hasegawa K, Naiki H, Yamada M (2005) Preformed β-amyloid fibrils are destabilized by coenzyme Q10 *in vitro*. *Biochem Biophys Res Commun* **330**, 111-116.

[15] Ono K, Hirohata M, Yamada M (2006) α-lipoic acid exhibits anti-amyloidogenicity for β-amyloid fibrils *in vitro*. *Biochem Biophys Res Commun* **341**, 1046-1052.
[16] Ronicke R, Klemm A, Meinhardt J, Schroder UH, Fandrich M, Reymann KG (2008) Aβ mediated diminution of MTT reduction–an artefact of single cell culture? *PLoS One* **3**, e3236.
[17] Hirohata M, Hasegawa K, Tsutsumi-Yasuhara S, Ohhashi Y, Ookoshi T, Ono K, Yamada M, Naiki H (2007) The anti-amyloidogenic effect is exerted against Alzheimer's β-amyloid fibrils *in vitro* by preferential and reversible binding of flavonoids to the amyloid fibril structure. *Biochemistry* **46**, 1888-1899.
[18] Bitan G, Kirkitadze MD, Lomakin A, Vollers SS, Benedek GB, Teplow DB (2003) Amyloid β-protein (Aβ) assembly: Aβ40 and Aβ42 oligomerize through distinct pathways. *Proc Natl Acad Sci U S A* **100**, 330-335.
[19] Abe K, Saito H (1998) Amyloidβ protein inhibits cellular MTT reduction not by suppression of mitochondrial succinate dehydrogenase but by acceleration of MTT formazan exocytosis in cultured rat cortical astrocytes. *Neurosci Res* **31**, 295-305.
[20] Szuts EZ, Harosi FI (1991) Solubility of retinoids in water. *Arch Biochem Biophys* **287**, 297-304.
[21] Bourdel-Marchasson I, Delmas-Beauvieux MC, Peuchant E, Richard-Harston S, Decamps A, Reignier B, Emeriau JP, Rainfray M (2001) Antioxidant defences and oxidative stress markers in erythrocytes and plasma from normally nourished elderly Alzheimer patients. *Age Ageing* **30**, 235-241.
[22] Foy CJ, Passmore AP, Vahidassr MD, Young IS, Lawson JT (1999) Plasma chain-breaking antioxidants in Alzheimer's disease, vascular dementia and Parkinson's disease. *QJM* **92**, 39-45.
[23] Jeandel C, Nicolas MB, Dubois F, Nabet-Belleville F, Penin F, Cuny G (1989) Lipid peroxidation and free radical scavengers in Alzheimer's disease. *Gerontology* **35**, 275-282.
[24] Jimenez-Jimenez FJ, Molina JA, de Bustos F, Orti-Pareja M, Benito-Leon J, Tallon-Barranco A, Gasalla T, Porta J, Arenas J (1999) Serum levels of β-carotene, α-carotene and vitamin A in patients with Alzheimer's disease. *Eur J Neurol* **6**, 495-497.
[25] Zaman Z, Roche S, Fielden P, Frost PG, Niriella DC, Cayley AC (1992) Plasma concentrations of vitamins A and E and carotenoids in Alzheimer's disease. *Age Ageing* **21**, 91-94.
[26] Goodman AB, Pardee AB (2003) Evidence for defective retinoid transport and function in late onset Alzheimer's disease. *Proc Natl Acad Sci U S A* **100**, 2901-2905.
[27] Perrig WJ, Perrig P, Stahelin HB (1997) The relation between antioxidants and memory performance in the old and very old. *J Am Geriatr Soc* **45**, 718-724.
[28] Corcoran JP, So PL, Maden M (2004) Disruption of the retinoid signalling pathway causes a deposition of amyloid β in the adult rat brain. *Eur J Neurosci* **20**, 896-902.
[29] Ding Y, Qiao A, Wang Z, Goodwin JS, Lee ES, Block ML, Allsbrook M, McDonald MP, Fan GH (2008) Retinoic acid attenuates β-amyloid deposition and rescues memory deficits in an Alzheimer's disease transgenic mouse model. *J Neurosci* **28**, 11622-11634.
[30] Dev S, Adler AJ, Edwards RB (1993) Adult rabbit brain synthesizes retinoic acid. *Brain Res* **632**, 325-328.
[31] McCaffery P, Drager UC (1994) Hot spots of retinoic acid synthesis in the developing spinal cord. *Proc Natl Acad Sci U S A* **91**, 7194-7197.
[32] Zelent A, Mendelsohn C, Kastner P, Krust A, Garnier JM, Ruffenach F, Leroy P, Chambon P (1991) Differentially expressed isoforms of the mouse retinoic acid receptor beta generated by usage of two promoters and alternative splicing. *EMBO J* **10**, 71-81.
[33] Ahlemeyer B, Krieglstein J (2000) Inhibition of glutathione depletion by retinoic acid and tocopherol protects cultured neurons from staurosporine-induced oxidative stress and apoptosis. *Neurochem Int* **36**, 1-5.
[34] Grundman M, Delaney P (2002) Antioxidant strategies for Alzheimer's disease. *Proc Nutr Soc* **61**, 191-202.
[35] Pardridge WM, Sakiyama R, Coty WA (1985) Restricted transport of vitamin D and A derivatives through the rat blood-brain barrier. *J Neurochem* **44**, 1138-1141.
[36] Werner EA, Deluca HF (2002) Retinoic acid is detected at relatively high levels in the CNS of adult rats. *Am J Physiol Endocrinol Metab* **282**, E672-E678.

Neurobiology of Disease

Stress Acts Cumulatively To Precipitate Alzheimer's Disease-Like Tau Pathology and Cognitive Deficits

Ioannis Sotiropoulos,[1]* Caterina Catania,[1]* Lucilia G. Pinto,[2] Rui Silva,[2] G. Elizabeth Pollerberg,[3] Akihiko Takashima,[4] Nuno Sousa,[2] and Osborne F. X. Almeida[1]

[1]Max Planck Institute of Psychiatry, 80804 Munich, Germany, [2]Life and Health Sciences Research Institute, University of Minho, Campus Gualtar, 4710-057 Braga, Portugal, [3]Developmental Neurobiology, Institute of Zoology, University of Heidelberg, 69120 Heidelberg, Germany, and [4]Laboratory for Alzheimer's Disease, RIKEN Brain Science Institute, 2–1 Hirosawa, Wako-shi, Saitama, Japan

Stressful life experiences are likely etiological factors in sporadic forms of Alzheimer's disease (AD). Many AD patients hypersecrete glucocorticoids (GCs), and their GC levels correlate with the rate of cognitive impairment and extent of neuronal atrophy. Severity of cognitive deficits in AD correlates strongly with levels of hyperphosphorylated forms of the cytoskeletal protein TAU, an essential mediator of the actions of amyloid β (Aβ), another molecule with a key pathogenic role in AD. Our objective was to investigate the sequential interrelationships between these various pathogenic elements, in particular with respect to the mechanisms through which stress might precipitate cognitive decline. We thus examined whether stress, through the mediation of GCs, influences TAU hyperphosphorylation, a critical and early event in the cascade of processes leading to AD pathology. Results from healthy, wild-type, middle-aged rats show that chronic stress and GC induce abnormal hyperphosphorylation of TAU in the hippocampus and prefrontal cortex (PFC), with contemporaneous impairments of hippocampus- and PFC-dependent behaviors. Exogenous GC potentiated the ability of centrally infused Aβ to induce hyperphosphorylation of TAU epitopes associated with AD and cytoplasmic accumulation of TAU, while previous exposure to stress aggravated the biochemical and behavioral effects of GC in Aβ-infused animals. Thus, lifetime stress/GC exposure may have a cumulative impact on the onset and progress of AD pathology, with TAU hyperphosphorylation serving to transduce the negative effects of stress and GC on cognition.

Introduction

The etiology of late-onset, sporadic (nonfamilial) forms of Alzheimer's disease (AD) is largely unknown, but there is growing consensus that lifetime events such as environmental stressors may increase the probability of risk for the disease (Wilson et al., 2003; Csernansky et al., 2006; Kang et al., 2007). This view is supported by reports of hypersecretion of stress hormones [glucocorticoids (GCs)] in AD patients (Hartmann et al., 1997; Weiner et al., 1997; Elgh et al., 2006), and indications that psychological distress may cause mild cognitive impairment (Wilson et al., 2003) and predispose affected individuals to AD (Wilson et al., 2007). Studies in humans and animals demonstrate a robust relationship among elevated GC secretion, cognitive impairment, and neuronal atrophy. The cognition-impairing actions of stress and high GC levels are largely ascribed to concomitant reductions in the volume of the hippocampus (Sousa et al., 2000; Landfield et al., 2007; Lupien et al., 2009), a brain area that displays some of the earliest neurodegenerative changes in AD. Stress and GC induce similar volumetric reductions in the prefrontal cortex (PFC) (Cerqueira et al., 2007; Schubert et al., 2008), which receives afferents from the hippocampus and is critical for the control of higher cognitive functions.

Amyloid β (Aβ) has a well established role in AD-associated neuropathology, although there is evidence that cognitive deficits are detectable in advance of Aβ deposition into senile plaques (Terry et al., 1991; Guillozet et al., 2003). Previous studies in mice carrying human transgenes implicated in familial AD reported that chronic stress and exogenous GC accelerate the production and deposition of Aβ and impair learning and memory (Green et al., 2006; Jeong et al., 2006); additionally, treatment of nontransgenic animals with either chronic stress or exogenous GC shifts the metabolism of amyloid precursor protein (APP) in favor of the amyloidogenic pathway (Catania et al., 2009). On the other hand, the cytoskeletal protein TAU appears to mediate the pathogenic actions of Aβ (Rapoport et al., 2002; Roberson et al., 2007) after its hyperphosphorylation by TAU kinases such as GSK3β and cdk5 (Takashima et al., 1998). Indeed, anomalous hyperphosphorylation of TAU is another pathogenic mechanism in AD: specifically, hyperphosphorylated TAU detaches from microtubules, oligomerizes, and accumulates in the somato-

Received Feb. 10, 2011; accepted Feb. 23, 2011.

Author contributions: I.S., C.C., N.S., and O.F.X.A. designed research; I.S., C.C., L.G.P., R.S., and N.S. performed research; A.T. contributed unpublished reagents/analytic tools; I.S., A.T., N.S., and O.F.X.A. analyzed data; I.S., G.E.P., A.T., N.S., and O.F.X.A. wrote the paper.

C.C. and I.S. were supported by the Max Planck Society and European Union (EU) Marie Curie Training Fellowships at University College, London. The work was supported by the German-Portuguese Luso-Alemas Program and the EU CRESCENDO Consortium (Contract FP6-018652). Dieter Fischer and Jutta Waldherr provided excellent technical assistance; Isabel Matos blind scored behavioral and histochemical data; and Drs. Peter Davies and Peter Seubert generously supplied monoclonal antibodies.

*I.S. and C.C. contributed equally to this study.

The authors declare no competing financial interests.

Correspondence should be addressed to Osborne F. X. Almeida, Max Planck Institute of Psychiatry, Kraepelinstrasse 2-10, 80804 Munich, Germany. E-mail: osa@mpipsykl.mpg.de.

DOI:10.1523/JNEUROSCI.0730-11.2011

 0270-6474/11/317840-08$15.00/0

dendritic compartment, resulting in neuronal dystrophy and degeneration and cognitive impairment (Grundke-Iqbal et al., 1986; Sengupta et al., 1998; Schneider et al., 1999).

The results of the present study in nontransgenic middle-aged rats show that stress and GC markedly compromise hippocampus-dependent reference memory and PFC-dependent behavioral flexibility and aggravate the behavioral effects of central infusions of $A\beta_{1-40}$. These behavioral impairments occur concomitantly with increased levels of TAU kinases and hyperphosphorylated TAU, thus suggesting a new cellular mechanism through which stress and GC interfere with the neurostructural correlates of behavior.

Materials and Methods

Animal procedures. Male Wistar rats, aged 14 months, were used in accordance with European Union Council Directive 86/609/EEC and local animal welfare regulations. Animals were housed four to five per cage under standard environmental conditions [temperature 22°C; relative humidity 70%; 12 h light/dark cycle (lights on at 6:00 A.M.); *ad libitum* access to food and water]. Subgroups ($n = 6–7$) were subjected to 1 month of chronic, unpredictable stress (Catania et al., 2009). Briefly, the stress paradigm involved random application of one of the following stressors, daily: hypertonic saline [9% NaCl, i.p., 1 ml/100 g of body weight (BW)], overcrowding for 1 h, placement in a confined environment (30 min), or placement on a vibrating/rocking platform (1 h). Animals were then subjected to a first behavioral testing (see below) before receiving intracerebroventricular infusions of either freshly solubilized $A\beta_{1-40}$ or vehicle (see below) over 14 d. Subgroups of animals received subcutaneous GC injections [dexamethasone, 300 μg/ml/kg BW delivered in an oily suspension (depot) (1:10 Fortecortin, (Merck) in sesame oil (Sigma)] for 14 d. Animals were subjected to a second behavioral test at the end of the various treatments. Efficacy of the stress paradigm was verified at autopsy: basal serum corticosterone levels were 54.7 ± 4.8 and 384.6 ± 65.9 ng/ml, respectively, in control and stressed rats ($p < 0.02$); net body mass gain/loss was -12.1 ± 2.1 g in stressed rats and $+6.1 \pm 1.3$ g in control animals ($p \leq 0.0001$); thymus weights were 4.3 ± 0.4 mg/kg BW in stressed animals and 7.6 ± 0.9 mg/kg BW control animals ($p < 0.01$).

Intracerebral infusions. Alzet miniosmotic pumps (delivering 0.5 μl/h over 14 d; model 2002, Charles River), filled and equilibrated with 4.2 nM $A\beta_{1-40}$ (American Peptide) or vehicle (sterile distilled water), were placed subcutaneously under anesthetic. Alzet Brain Infusion sets were used to connect the outlet of the pumps to a cannula placed under stereotaxic control into a left lateral ventricle of the brain (stereotaxic coordinates: anteroposterior, −1.0 mm; dorsoventral, −2.5 mm; and mediolateral, +1.5 mm (right) with bregma as a reference, under pentobarbital (50 mg/kg) anesthesia. We infused $A\beta_{1-40}$ rather than the more pathogenic $A\beta_{1-42}$ species because the former aggregates less readily (Harper et al., 1997). None of the biometric parameters were significantly altered by the $A\beta_{1-40}$ infusions.

Behavioral tests. Spatial reference memory was tested using the Morris water maze over 4 consecutive days (4 trials per day). As previously described (Cerqueira et al., 2007), testing was conducted in a circular black tank (170 cm diameter) filled to a depth of 31 cm with opaque water (22°C) and placed in a dimly lit room with extrinsic clues. The tank was divided into virtual quadrants and had a black platform (12 cm diameter, at a height of 30 cm) placed in one of them. Data were collected using a video tracking system (Viewpoint). Assessment of reversal learning (four trial paradigm) was begun 1 d later using the above setup. For this, the escape platform was repositioned in the opposite (new) quadrant; and rats were tested in a four trial paradigm (1 trial per day), with distance and time spent swimming in each quadrant being recorded.

Immunocytochemistry. Half of each brain was used for immunohistochemical analysis; hippocampi and PFCs from the contralateral side were processed for Western blotting. Brains excised at autopsy were snap frozen, post-fixed in 4% paraformaldehyde, immersion fixed for 48 h, paraffin embedded, and sectioned at 8 μm. Following antigen retrieval (microwaved in sodium citrate, 30 min), washing (TBS), and blocking endogenous peroxides with H_2O_2 (3%), slide-mounted sections were

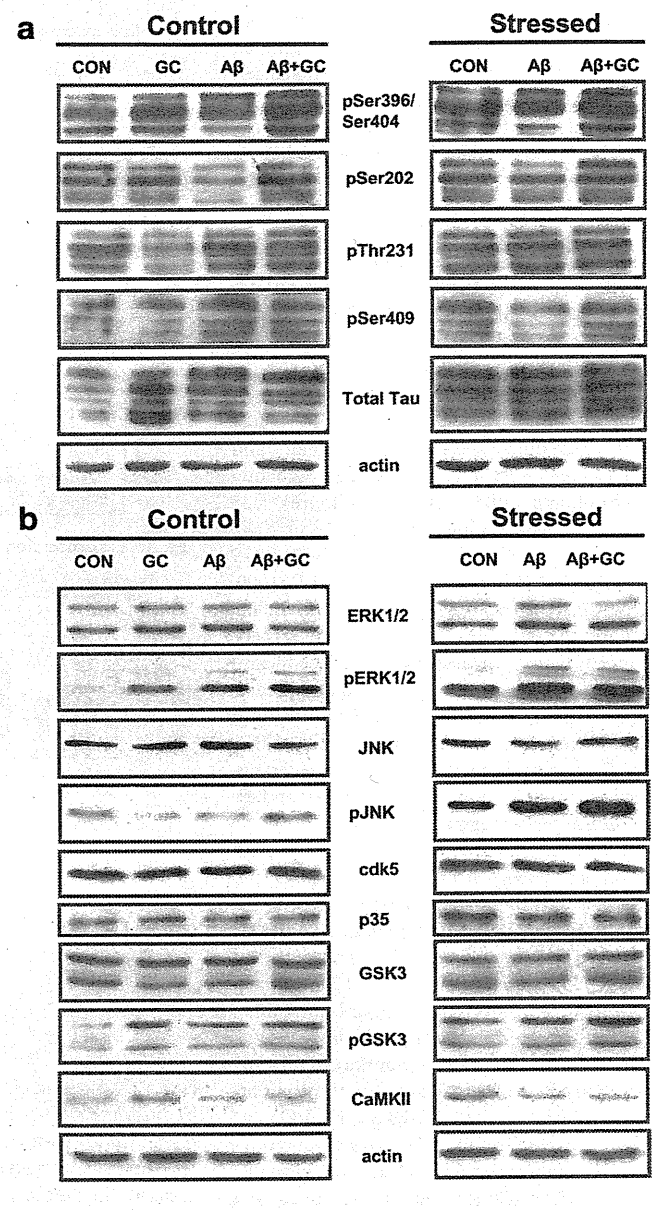

Figure 1. Chronic stress upregulates the expression of various phospho-TAU epitopes and TAU kinases. ***a***, ***b***, Depicted are representative immunoblots using a panel of phosphorylation-dependent TAU antibodies (***a***) and total and active isoforms of kinases (***b***).

incubated in an appropriate nonimmune serum (1:10 in TBS, pH 7.6, 30 min). Sections were then incubated [room temperature (RT) overnight] with primary antibodies of interest [Tau-5 (1:200), CP-13, PHF1, PG5 (all at 1:50), and 12E8 (1:100)] before washing and incubation with biotinylated secondary antibody (BioGenex) (RT, 30 min.) After a further wash in TBS, slides were incubated (30 min, RT) with a horseradish peroxidase complex (BioGenex). Immunopositive structures were revealed with the chromogen diaminobenzidine (1 mg/ml in 0.01% H_2O_2); stain development was monitored using a microscope. Negative controls were performed by omitting the primary antibody (no staining was seen in any sections). Staining was scored by visual examination on a scale of 0.5–5 by an independent investigator who was blind to the treatments. The degree of antibody staining was scored by visual examination on a scale of 0.5–5 by two independent subjects who were blind to the treatments.

Western blotting. Frozen hippocampi and PFC were homogenized in lysis buffer [100 mM Tris-HCl, 250 mM NaCl, 1 mM EDTA, 5 mM MgCl2, 1% NP-40, Complete Protease Inhibitor (Roche), and Phosphatase Inhibitor Cocktails I and II (Sigma)] using a Dounce glass homogenizer; extracts were cleared by centrifugation (14,000 × *g*), and their protein contents were estimated (Lowry assay) after reconstitution in Laemmli

buffer (250 mM Tris-HCl, pH 6.8, containing 4% SDS, 10% glycerol, 2% b-mercaptoethanol, and 0.002% bromophenol blue). Thereafter, lysates were electrophoresed on 10% acrylamide gels, and transferred onto nitrocellulose membranes (Protran BA 85, Schleicher & Schuell). Membranes were blocked in Tris-buffered saline containing 5% nonfat milk powder and 0.2% Tween-20 before incubation with the following antibodies: Tau-5 (1:200, BD Biosciences), CP-13 (p-Ser202-Tau), CP-9 (p-Thr231-Tau), PHF1 (p-Ser396/404-Tau), or PG5 (p-Ser409-Tau), all kindly provided Dr. Peter Davies (Albert Einstein College of Medicine, New York, NY) and used at a dilution of 1:50, total and *p*-Thr202/204 ERK1/2 (1:2500, Cell Signaling Technology), total and *p*-Thr183/Tyr185 JNK (1:1000, Cell Signaling Technology), cdk5 (1:1000, Millipore), p35 (Santa Cruz Biotechnology), GSK3β (1:2000, Santa · Cruz Biotechnology), *p*-Tyr216/279 GSK3β (1:2000, Biosource), CaMKII (1:1000, Cell Signaling Technology), and actin (1:2000, Millipore). Antigens were revealed by enhanced chemiluminescence (GE Healthcare) after incubation with appropriate horseradish peroxidase–IgG conjugates (GE Healthcare); blots were scanned and quantified using TINA 3.0 bioimaging software (Raytest) after ascertaining linearity. All values were normalized and expressed as percentages of control.

Detection of detergent-insoluble TAU. Sarkosyl-insoluble fractions from tissue protein extracts were prepared as previously described (Kimura et al., 2010). Briefly, frozen hippocampi of P301L tau mice were homogenized in Tris-buffered saline (10 mM Tris, 150 mM NaCl, pH 7.4) containing protease inhibitors (1 mg/ml antipain, 5 mg/ml pepstatin, 5 mg/ml leupeptin, 2 mg/ml aprotinin, and 0.5 mM 4-[2-aminoethyl]benzenesulfonyl fluoride hydrochloride) and phosphatase inhibitors (1 mM NaF, 0.4 mM Na_3VO_4, and 0.5 mM okadaic acid). After centrifugation, the supernatant was retained and Sarkosyl-insoluble, paired helical filament-enriched fractions were prepared from TBS-insoluble pellets after rehomogenization in 5 volumes of sucrose buffer (0.8 M NaCl, 10% sucrose solution including protease and phosphatases inhibitors as mentioned above) and centrifugation (100,000 × *g*, 20 min). Sarkosyl (10%) was added to the supernatant (1:10 v/v), and, after incubation at 37°C (1 h) and centrifugation (150,000 × *g*, 1 h), the resulting pellet was considered as the Sarkosyl-insoluble fraction. TBS-soluble and Sarkosyl-insoluble materials were solubilized in Laemmli sample buffer and subjected to SDS-PAGE and Western blot analysis using rabbit polyclonal anti-TAU (phosphorylated and nonphosphorylated isoforms) as described previously (Kimura et al., 2010).

Statistical analysis. With the exception of the reference memory test data (repeated-measures ANOVA), all data were evaluated by one-way ANOVA and appropriate *post hoc* pairwise tests using SPSS and SigmaStat (Systat) software packages; differences were considered to be significant if $p < 0.05$.

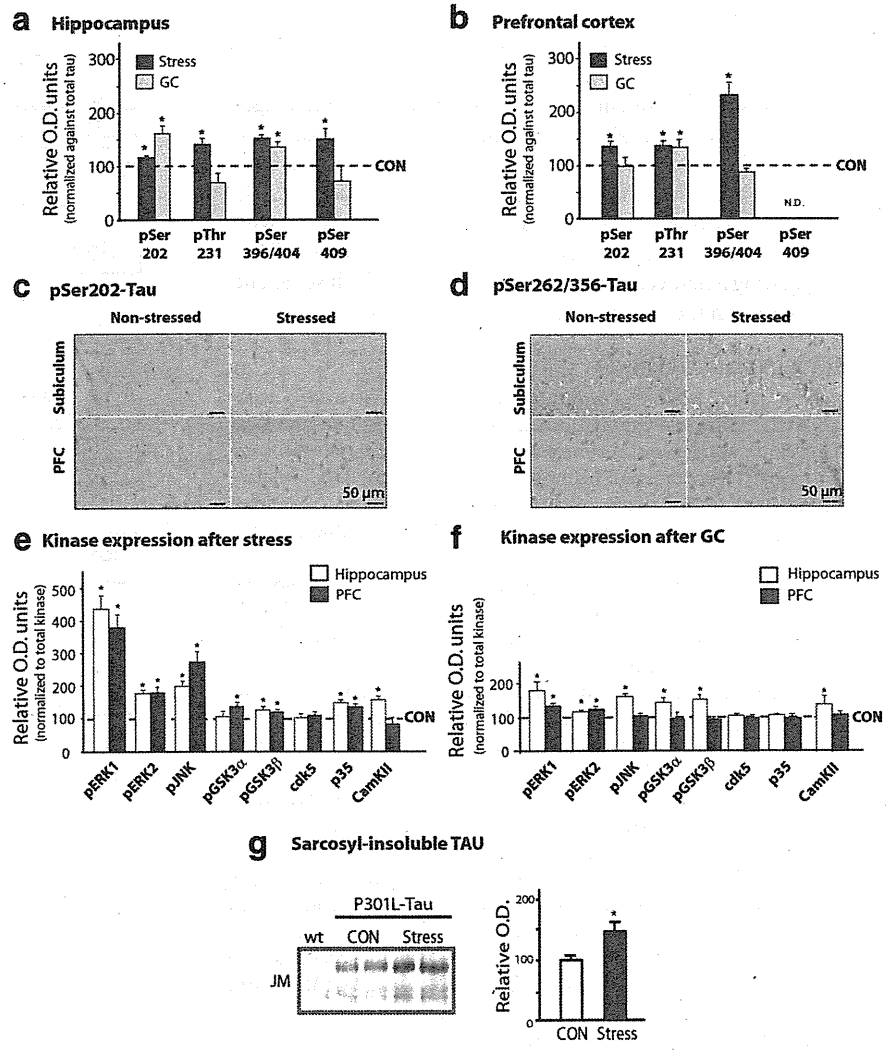

Figure 2. Stress and GCs induce TAU hyperphosphorylation in the hippocampus and PFC. TAU phosphorylation profiles in the hippocampus and PFC of chronically stressed or GC-treated rats were monitored by Western immunoblotting and immunocytochemistry. ***a***, ***b***, Western blot analysis of TAU phosphorylation at different epitopes in hippocampus and PFC. TAU phosphorylation levels were normalized against total TAU levels (recognized by TAU-5); control (CON) animals are shown as dotted lines (100%). ***c***, ***d***, Immunohistochemical staining of pSer202-TAU and pSer262/356-TAU, in the hippocampus (subiculum) and PFC, using antibodies CP-13 and 12E8 antibodies, respectively. Immunoreactive signals were confined to the cell bodies of pyramidal neurons. ***e***, ***f***, Both stress and GCs increased the expression of a number of kinases in the hippocampus and PFC of animals exposed to stress or GC, compared with controls. For all phosphorylated forms of kinases, data were normalized with respect to total levels of the respective kinase. ***g***, Western blot analysis of sarkosyl-insoluble fractions from P301L-TAU animals showing that chronic stress increases the levels of sarcosyl-insoluble TAU. All numerical data shown represent mean ± SEM values ($N = 7$), depicted with respect to data obtained in control tissues. *Significant differences from CON values ($p \leq 0.05$).

Results

Chronic stress and GC induce abnormal hyperphosphorylation of TAU

Abnormal hyperphosphorylation of tau is a critical event in the cascade leading to AD pathology (Grundke-Iqbal et al., 1986; Schneider et al., 1999; Kimura et al., 2007). Clinical reports of GC hypersecretion in AD patients and in cases of mild cognitive impairment, a condition with a high conversion rate to AD (Hartmann et al., 1997; Weiner et al., 1997; Elgh et al., 2006; Wilson et al., 2007), prompted us to examine how elevated GC secretion, induced by chronic unpredictable stress, influences the pattern of tau phosphorylation in the hippocampus and PFC, brain regions that are established targets of the deleterious morphological and behavioral actions of stress and GC (Sousa et al., 2000; Cerqueira et al., 2007; Schubert et al., 2008; Sotiropoulos et al., 2008a) and among the first to show signs of AD neuropathology (Lace et al., 2009).

Immunoblot analysis showed that chronic stress results in hyperphosphorylation of TAU at pSer202, pThr231, pSer396/404, and pSer409 in both brain regions of interest ($p \leq 0.05$ in all cases) (Figs. 1, 2*a*,*b*); immunocytochemical confirmation of these

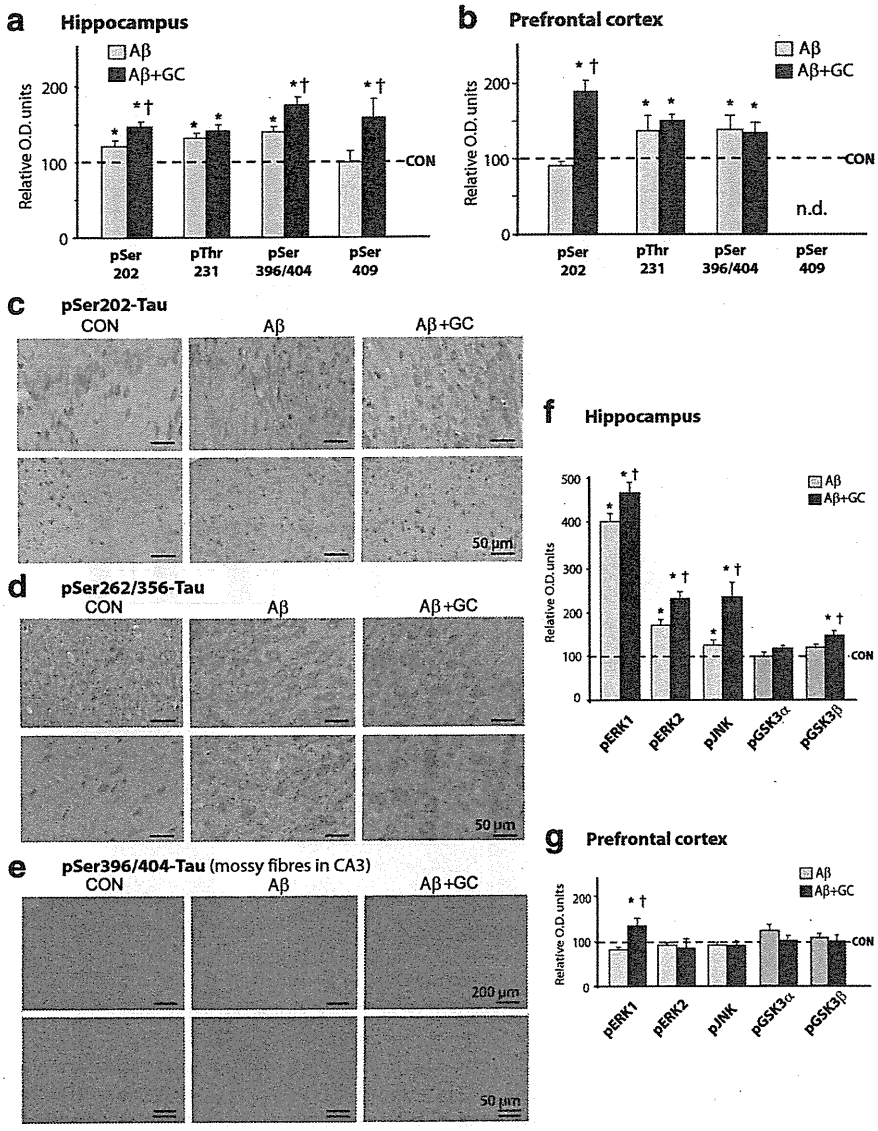

Figure 3. GCs potentiate Aβ-induced TAU hyperphosphorylation. ***a***, ***b***, Concomitant administration of Aβ and GCs resulted in increases in the levels of several phospho-TAU isoforms in the rat hippocampus (***a***) and PFC (***b***), as measured by Western blotting; these increases were greater than after treatment with Aβ alone ($^{\dagger}p \leq 0.05$). Note the differential responses of the hippocampus and PFC in terms of number of phospho-TAU epitopes that were affected by the combined Aβ + GC treatment. ***c***, ***d***, Immunocytochemical analysis of pSer202-TAU (detected with antibody CP13; ***c***) and pSer262/356-TAU (antibody 12E8; ***d***) in hippocampus (subiculum) and PFC confirmed the above Western blot analysis data. ***e***, Illustration of pSer396/404-TAU staining (using antibody PHF-1) in the mossy fiber system of control rats and rats treated with Aβ or Aβ + GCs. While CP-13 and 12E8 immunoreactivity was localized to neuronal perikarya, that of PHF-1 was predominantly found within mossy fibers. ***f***, Significant increases in the expression of pERK1/2, pJNK and pGSK3β levels were observed in the hippocampus. Note that total levels of the respective TAU kinases were not altered by any of the treatments. Numerical data represent mean ± SEM values ($N = 7$), depicted after normalization to total Tau (***a***, ***b***) or respective total kinases (***f***, ***g***). *Significant differences from CON values ($p \leq 0.05$); †significant difference ($p \leq 0.05$) between corresponding pairs of values for each treatment group (Aβ vs Aβ + GC).

results using the phosphorylation-dependent antibodies CP13 (pSer202-TAU) and 12E8 (pSer262/Ser356-TAU) are shown for the subiculum (Fig. 2*c*) and PFC (Fig. 2*d*). Importantly, administration of exogenous GC to nonstressed animals largely reproduced the effects of chronic stress ($p < 0.05$ in all cases) (Figs. 1, 2*a*,*b*). In addition to monitoring TAU phosphorylation profiles, we also examined several kinases implicated in TAU pathology associated with AD (Mazanetz et al., 2007). As shown in Figures 1 and 2, *e* and *f*, stress and/or GC activated pERK1/2, pGSK3β, p35 (the cdk5 activator), pJNK, and CaMKII in the hippocampus and PFC ($p \leq 0.05$). Together, these results show that stress and GC promote a pattern of changes that closely resembles neuropathological findings in AD and in cellular and animal models of the disease (Green et al., 2006; Jeong et al., 2006 Sotiropoulos et al., 2008b).

Since the expression of hyperphosphorylated TAU species correlates with the presence of insoluble TAU aggregates in AD brains (Wang et al., 1995; Alonso et al., 2001; Maeda et al., 2006), we next examined whether stress influences the aggregation of TAU. To that end, Sarkosyl-insoluble TAU was extracted from the brains of aggregation-prone P301L-Tau transgenic mice (Kimura et al., 2010) and analyzed by Western blotting. Expectedly (Kimura et al., 2010), brains from P301L-Tau mice showed detectable levels of detergent-insoluble TAU immunoreactivity; the latter was significantly increased in extracts from P301L-Tau mice that had been previously exposed to stress (Fig. 2*g*). These results indicate that stress aggravates TAU aggregation.

Potentiating effects of glucocorticoids

GCs were recently shown to stimulate the generation of Aβ in experimental animals (Green et al., 2006; Jeong et al., 2006; Catania et al., 2009) and neural cell cultures (Sotiropoulos et al., 2008b) and to potentiate the deleterious effects of Aβ on neuronal survival (Sotiropoulos et al., 2008b). Demonstrations that GCs trigger hyperphosphorylation of TAU in neuronal cultures (Sotiropoulos et al., 2008b) raised the question of whether this is also the case *in vivo*. We addressed this by monitoring the expression of pathogenically relevant phospho-TAU epitopes (Augustinack et al., 2002; Ewers et al., 2007; van der Vlies et al., 2009) in a nontransgenic rat model of early-stage AD (Stéphan and Phillips, 2005).

Chronic intracerebroventricular infusions of Aβ led to a significant increase in the expression of the majority of tested phosphorylated sites of tau protein in the hippocampus and PFC ($p \leq 0.05$) (Fig. 3*a*,*b*), indicating tau hyperphosphorylation at different sites. These effects were potentiated by concomitant treatment with GCs, in particular with respect to pSer202-TAU in the hippocampus (Fig. 3*a*,*c*) and PFC (Fig. 3*b*), pSer396/404- and pSer409-TAU in the hippocampus (Fig. 3*a*), and pSer262/356 in the PFC (Fig. 3*d*). In addition, the combined treatment of GC and Aβ resulted in increased pSer396/404-TAU staining of the hippocampal mossy fiber network (GC+Aβ > Aβ alone) (Fig. 3*e*). Correspondingly, compared with Aβ alone, the combined Aβ and GC treatment regimen resulted in a greater upregulation of hippocampal levels of activated ERK1/2, pJNK, and pGSK3β ($p \leq 0.05$ in all cases) (Fig. 3*f*).

History of stress increases sensitivity to GC and Aβ

Individuals experience multiple lifetime stressors, usually with an amplification of the GC response to successive stressful episodes

(Lupien et al., 2009). In an attempt to simulate this natural situation, middle-aged rats were subjected to chronic stress before receiving intracerebroventricular infusions of Aβ and/or peripheral GC injections.

Compared with animals that received Aβ alone, those receiving the combinatorial treatment of Aβ and GC showed an enhancement of phosphorylation of several TAU sites (pSer202, pSer396/404, pThr231, pSer409) in the PFC and hippocampus (Fig. 4*a*,*b*), with parallel increases in pERK1/2, pJNK, and pGSK3β (Fig. 4*c*,*d*) expression. In agreement with these findings, stressed animals that were subsequently treated with Aβ and GC displayed more intense immunostaining of PHF-1 (pSer396/404-TAU) in hippocampal neurons compared with those treated with Aβ alone (Fig. 4*e*). Furthermore, GC led to a greater accumulation of hyperphosphorylated TAU in the perikarya of hippocampal (compare Figs. 4*e*, 3*e*) and PFC (Fig. 4*f*) neurons of previously stressed animals (stress + GC + Aβ > GC+ Aβ); these findings are supported by the observation of graded increases in the level of total neuronal TAU detected with pan-TAU (TAU-5) antiserum (Table 1).

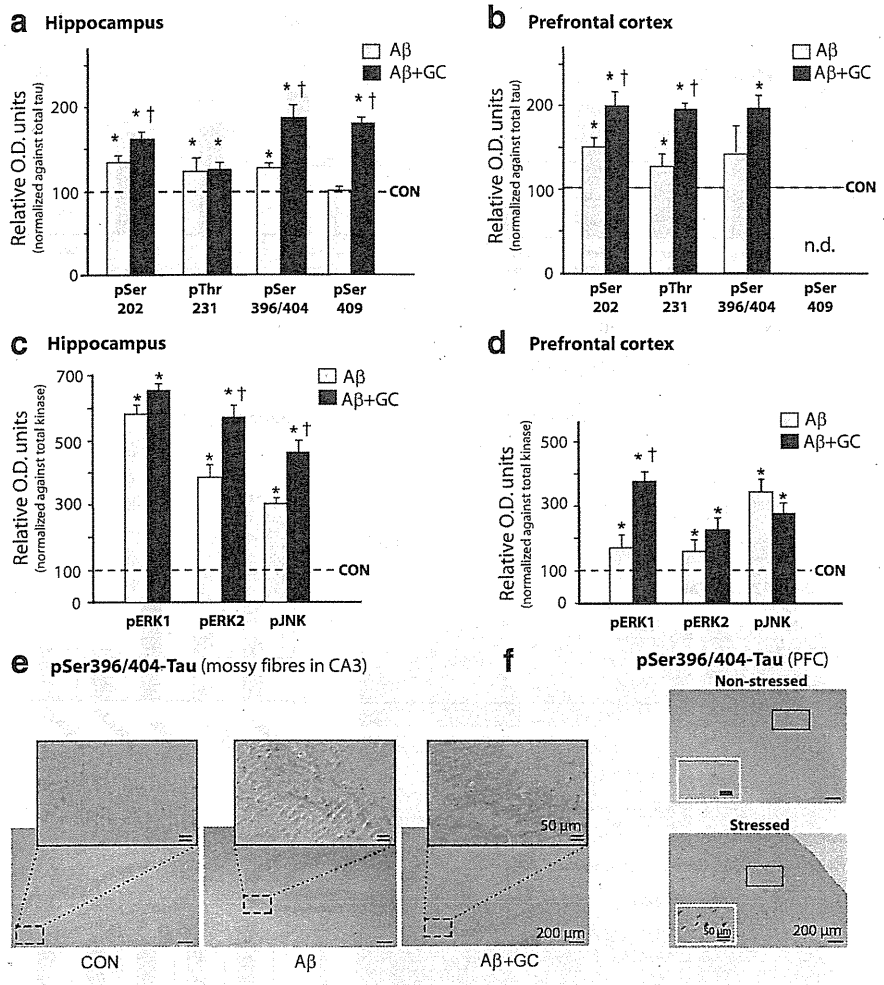

Figure 4. Previous stressful experience increases sensitivity to Aβ + GC. ***a–d***, Animals that had experienced chronic unpredictable stress (1 month) responded to cotreatment with dexamethasone GCs, 300 μg/kg BW/d) and Aβ (0.3 nmol/d) with increases in TAU phosphorylation (***a***, ***b***) and levels of TAU-related kinases (***c***, ***d***); overall, stressed animals exhibited higher susceptibility to the combinatorial treatment than nonstressed animals. Immunoblotting revealed that, in contrast to the hippocampus, the PFC of previously stressed animals show a greater extent of TAU hyperphosphorylation (compare Fig. 2*b*) and expression of active forms of ERK1/2 and JNK (compare Figs. 4*c*,*d*, 3*f*,*g*) after treatment with GC + Aβ, indicating the cumulative nature and dissipation of the effects of stress and GCs from the hippocampus to the PFC. ***e***, Immunohistochemical analysis demonstrated an enhancement of PHF-1 immunoreactivity in the mossy fiber network of the hippocampus of stressed rats receiving Aβ or Aβ + GC (Aβ + GC > Aβ > vehicle). ***f***, Strong PHF-1 immunoreactivity is shown in the perikarya of PFC neurons of stressed + Aβ + GC-treated rats (micrograph of the PFC region from a nonstressed rat that had been treated with Aβ + GC is shown in panel ***f***, for comparison). Insets in ***f*** are high-power magnifications of the rectangular areas marked in the respective low-magnification micrographs. All numerical data shown represent mean ± SEM values ($N = 6–7$), depicted with respect to data obtained in control tissues (CON, dotted line), set at 100%. *Significant differences from CON values ($p \leq 0.05$); †Significant difference ($p \leq 0.05$) between corresponding pairs of values for each treatment group (stress + Aβ vs stress + Aβ + GC).

Behavioral profiles

There is a strong correlation between the extent of TAU hyperphosphorylation and the severity of impairments of memory, speed of mental processing, and executive functions in humans (Augustinack et al., 2002; Ewers et al., 2007; Lace et al., 2009); in experimental animals, learning and memory are impaired when TAU is hyperphosphorylated (Gatz et al., 2006; Kimura et al., 2007).

Consistent with previous findings (Sousa et al., 2000; Cerqueira et al., 2007), tests of hippocampus-dependent spatial reference memory and PFC-dependent reversal learning showed that both stress and GC disturbed hippocampus-dependent reference memory ($p < 0.05$) (Fig. 5*a*,*b*) and PFC-dependent behavioral flexibility ($p < 0.05$) (Fig. 5*c*,*d*). Central infusions of Aβ significantly impaired reference memory ($p < 0.001$) (Fig. 5*a*), an effect aggravated by coadministration of GC. As is evident from Figure 5*b*, even more pronounced impairments of reference memory were observed when Aβ and GC were applied to animals that had been previously exposed to stress (stress + Aβ vs stress + Aβ + GC, $p < 0.0001$). Behavioral flexibility was impaired by centrally applied Aβ ($p < 0.001$) (Fig. 5*c*). Interestingly, superimposition of GC did not worsen this PFC-dependent behavioral parameter (Fig. 5*c*), matching the lack of changes in TAU phosphorylation in the PFC after the combined treatment (Fig. 2*b*). On the other hand, GC significantly exacerbated this PFC-dependent behavioral deficit in previously stressed animals ($p < 0.05$ (Fig. 4*d*). Together with the data on the hyperphosphorylation and accumulation of TAU (compare Figs. 3, 4) (Table 1), these findings highlight the cumulative and deleterious effects of stress/GCs.

Discussion

Environmental factors account for 25–40% of the risk of developing AD (Gatz et al., 2006), a disease that develops progressively over decades. Stress, whose effects are mediated by GCs, is a plausible causal agent (Wilson et al., 2003; Csernansky et al., 2006; Kang et al., 2007). Clinical studies show a relationship between GC levels and severity of symptoms (Miller et al., 1998) and suggest that high GC levels accelerate disease progression (Csernansky et al., 2006).

The present study in rats delivers new insights into the link between stress and AD. Our results show that stress induces a biochemical anomaly found in AD, namely, hyperphosphorylation of the microtubule protein TAU; importantly, at least two of

Table 1. Relative amounts of TAU staining in the hippocampus (CA3 subfield) and PFC of control and stressed animals treated with either vehicle, Aβ or Aβ and GC

	Hippocampal CA3	PFC
Control		
Vehicle	++	+
Aβ	+++	+
Aβ + GCs	++++	++
Stress		
Vehicle	++	++
Aβ	+++	+++
Aβ + GCs	+++++	+++++

Total TAU was detected using TAU-5, and scores were assigned by an observer who was blind to the treatments. +, Very low; ++, low; +++, moderate; ++++, high; +++++, very high.

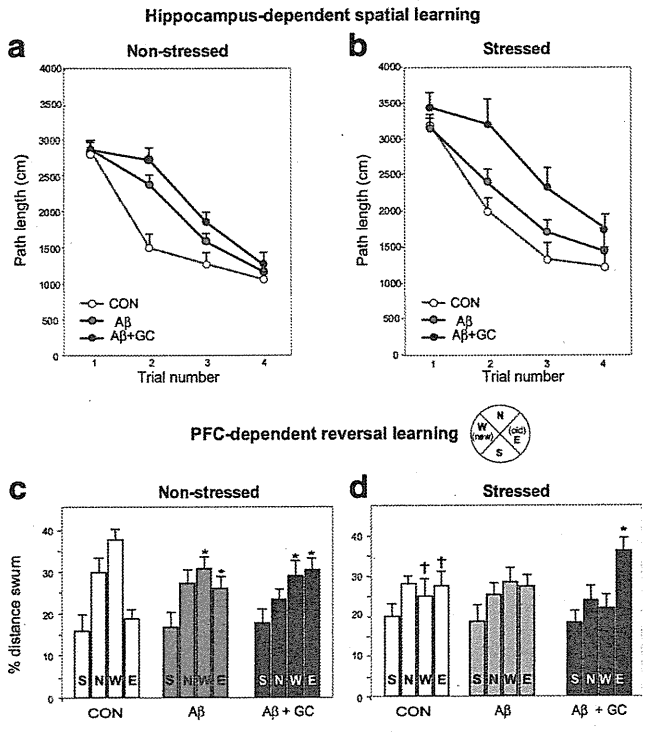

Figure 5. Stress exacerbates the cognition-impairing actions of Aβ and GC. ***a–d***, Hippocampus-dependent spatial reference memory (***a***, ***b***) and PFC-dependent working memory (reversal learning used to measure behavioral flexibility) (***c***, ***d***) in nonstressed (***a***, ***c***; $N = 7$) and stressed (***b***, ***d***; $N = 6$) rats. Chronic, unpredictable stress (1 month) was imposed before subgroups of animals were treated with either vehicle, Aβ or Aβ+GC for 14 d. $A\beta_{1-40}$ was chronically infused into the lateral ventricle at a dose of 0.3 nmol/d; dexamethasone (GC) was given as a daily depot injection at a dose of 300 μg/kg, s.c. In nonstressed animals, spatial reference memory was impaired after Aβ treatment ($p < 0.001$), and concomitant GC administration resulted in slight worsening of the deficit (***a***). While treatment with Aβ alone did not interfere with spatial memory in previously stressed rats, combined treatment with Aβ and GC markedly impaired spatial memory ($p < 0.0001$) (***b***). Compared with their nonstressed counterparts, stressed rats showed deficits in working memory ($p < 0.05$), as revealed by comparison of percentage distance swum in the new (W) and old (E) quadrant of the maze (***c***, ***d***). Treatment of nonstressed rats with Aβ reduced performance in the reversal learning test ($p < 0.05$), an effect that was not changed in GC + Aβ-treated animals (***c***). In contrast, although reversal learning was not disrupted after administration of Aβ alone to previously stressed animals, the behavior was significantly impoverished in stressed animals that were subsequently given the combined Aβ + GC regimen ($p < 0.05$) (***d***). *Significant differences from CON values; †significant difference between stressed and nonstressed animals.

the phospho-TAU epitopes (pThr231 and pSer262) upregulated by stress are strongly implicated in the neuropathology of AD (Grundke-Iqbal et al., 1986; Sengupta et al., 1998; Kimura et al., 2007; Mazanetz and Fischer, 2007; Wang et al., 2007; Sotiropoulos et al., 2008b). Hyperphosphorylation of Thr231- and Ser262-

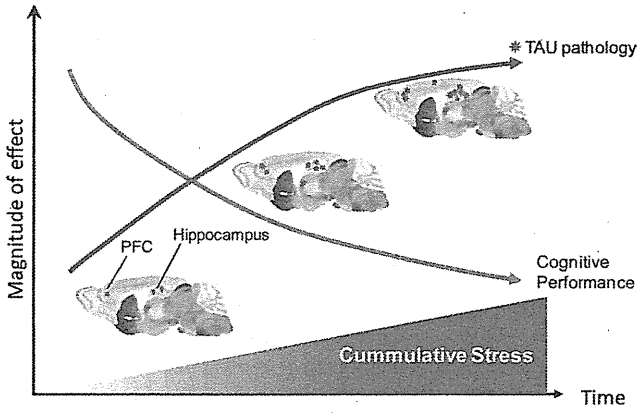

Figure 6. Working model of how stress acts cumulatively to induce TAU pathology and cognitive impairment. Repeated exposures to adverse life events (stress), accompanied by increased levels of GCs, induce TAU pathology in a cumulative manner. TAU hyperphosphorylation is probably stimulated secondarily to stress/GC-induced misprocessing of APP to amyloidogenic peptides such as amyloid β and C99 (Sotiropoulos et al., 2008a; Catania et al., 2009). Hyperphosphorylated TAU accumulates and aggregates in neuronal perikarya, leading to neuronal dystrophy and dysfunction. The first detrimental signs of stress are seen in the hippocampal and parahippocampal regions, gradually spreading to the PFC and other cortical regions; similar spatiotemporal patterns are observed in patients with Alzheimer's disease (Lace et al., 2009). Rat brain images were adapted from Swanson (1999).

TAU disrupts microtubule stability and leads to retrograde neuronal degeneration and synaptic loss; moreover, strong associations between increased levels of pThr231 and pSer262 and the appearance of neurofibrillary tangles have been reported previously (Sengupta et al., 1998; Schneider et al., 1999; Alonso Adel et al., 2006; Kimura et al., 2007; Mazanetz and Fischer, 2007). We here found that administration of exogenous GCs to middle-aged rats partly recapitulates the effects of stress on TAU hyperphosphorylation. Although specific TAU phosphoepitopes were differentially regulated by stress and GCs, the overall results obtained here and in earlier *in vitro* studies (Sotiropoulos et al., 2008b) clearly implicate GCs as a key mediator of the cellular response to stress. Nevertheless, contributions by other stress-related molecules such as corticotrophin-releasing hormone cannot be excluded (Rissman et al., 2007), and possible interactions between GC and catecholamines cannot be dismissed since stress stimulates the release of central norepinephrine (Nisenbaum et al., 1991). Understanding these interactions would be important given that TAU hyperphosphorylation and pathology is triggered by misprocessing of APP into Aβ and/or C99 (Takashima et al., 1998; Ghosal et al., 2009, Shipton et al., 2011) and that norepinephrine can reduce Aβ pathology (Heneka et al., 2010). Notwithstanding likely "ceiling effects" of the treatments (for the case of GC, see Green et al., 2006), physiological regulatory loops might also underpin our observations that the magnitude of effects of the combined treatments (e.g., stress and Aβ + GC) on TAU pathology are not merely additive.

The present finding that stress and GCs increase TAU hyperphosphorylation and accumulation in neuronal soma largely echoes and extends previous reports in AD transgenic models (Green et al., 2006; Jeong et al., 2006) and neuronal cell cultures (Sotiropoulos et al., 2008b). Specifically, our results show that stress/GCs induce extensive hyperphosphorylation of TAU at more epitopes (several considered critical in AD) than were described by Jeong et al. (2006); further, we show that stress aggravates the aggregation of Sarkosyl-insoluble TAU. Detergent-insoluble TAU aggregates eventually give rise to the neurofibrillary tangles characteristic of tauopathies, including AD (Wang et al., 1995; Kimura et al., 1996; Alonso et al., 2001); moreover, insoluble TAU and TAU oligomers are causally implicated in neurodegenerative processes (Berger et al., 2007) and

are found during presymptomatic stages of AD (Maeda et al., 2006). The discrepancy between our results (stress/GC-induced TAU hyperphosphorylation) and those of Green et al. (2006) may be attributed to the fact that the latter authors used 3×Tg mice expressing the P301-mutated TAU; wild-type TAU and P301L-mutated TAU display distinct phosphorylation profiles and exert dissimilar effects on neuronal structure and function (Kimura et al., 2010) and may be differentially regulated by stress. Further, Green et al. (2006) studied whole-brain homogenates, whereas our analysis in wild-type animals focused on specific brain regions that are affected in AD and targeted by stress/GCs.

Dendritic and synaptic atrophy, as well as cognitive impairments, are well known consequences of chronic stress and the accompanying increases in GC secretion (Sousa et al., 2000; Cerqueira et al., 2007; Landfield et al., 2007; Schubert et al., 2008; Lupien et al., 2009), albeit through still poorly understood cellular mechanisms. Extending earlier reports on the deleterious effects of GCs on cytoskeletal proteins, including TAU (Stein-Behrens et al., 1994; Cereseto et al., 2006), the results of the present study demonstrate that stress and GCs induce TAU hyperphosphorylation at epitopes implicated in cytoskeletal pathology and synaptic loss in AD patients (e.g., pSer262) (Callahan et al., 2002; Lauckner et al., 2003) and correlated with hippocampal atrophy in AD patients (e.g., pThr231) (Hampel et al., 2005). Clinical studies report a strong correlation between the extent of TAU hyperphosphorylation (including that of the Thr231 and Ser262 residues) and severity of impairments of memory, speed of mental processing, and executive functions (Augustinack et al., 2002, Ewers et al., 2007; van der Vlies et al., 2009). In addition, TAU hyperphosphorylation is associated with synaptic loss and memory impairment in experimental animals (Kimura et al., 2007). Based on the above considerations, we suggest that TAU hyperphosphorylation might be part of the cellular mechanism through which stress and GCs cause dendritic and synaptic dysfunction. In this connection, it is relevant to mention that recently Hoover et al. (2010) showed that hyperphosphorylated TAU within dendritic spines induces synaptic abnormalities, while Ittner et al. (2010) demonstrated that TAU mediates the synaptotoxic actions of Aβ. Results of the present study, together with other reports that TAU is essential for the manifestation of the actions of Aβ (Busciglio et al., 1995; Rapoport et al., 2002; Roberson et al., 2007; Shipton et al., 2011) and our previous demonstrations that stress and GCs trigger APP misprocessing in animals (Catania et al., 2009) and neuronal cultures (Sotiropoulos et al., 2008b), provide a mechanistic sequence through which stress leads to the expression of AD-relevant biochemical and behavioral markers. Accordingly, Aβ and TAU are introduced as new players in the cascade of events responsible for stress-induced brain dysfunction.

There is growing consensus that stress renders individuals vulnerable to brain disorders by causing inappropriate remodeling of individual neurons and disconnection of critical neural circuits (Cerqueira et al., 2007; Sotiropoulos et al., 2008a). The results reported here show that animals with a history of stress are more sensitive to the deleterious actions of Aβ and GCs; moreover, previously stressed animals express higher levels of hyperphosphorylated TAU and display more overt signs of memory dysfunction. Thus, previous stressful experiences may leave a "trace of vulnerability" to the development of AD-like pathology, with vulnerability increasing with age (Sotiropoulos et al., 2008a). In addition, our findings that GCs and stress act cumulatively suggest that repeated adverse experiences over an individual's lifetime will increase the probability or severity of AD pathology (Fig. 6). Our demonstration that stress and GCs can induce TAU pathology in otherwise healthy, middle-aged nontransgenic animals reinforces the view that lifetime experience may be an etiological factor in sporadic forms of AD. In this respect, the growing body of evidence for epigenetic regulation of AD pathophysiology (for review, see Chouliaras et al., 2010) is worth noting. Last, the introduction of TAU into the cascade of events leading to stress-induced neuronal and behavioral dysfunction has implications that extend beyond AD itself: stress is considered to be a major trigger of major depression, a disease that places individuals at a significant risk for developing AD (Ownby et al., 2006; Sun et al., 2008).

References

Alonso A, Zaidi T, Novak M, Grundke-Iqbal I, Iqbal K (2001) Hyperphosphorylation induces self-assembly of tau into tangles of paired helical filaments/straight filaments. Proc Natl Acad Sci U S A 98:6923–6928.

Alonso Adel C, Li B, Grundke-Iqbal I, Iqbal K (2006) Polymerization of hyperphosphorylated TAU into filaments eliminates its inhibitory activity. Proc Natl Acad Sci U S A 103:8864–8869.

Augustinack JC, Schneider A, Mandelkow EM, Hyman BT (2002) Specific TAU phosphorylation sites correlate with severity of neuronal cytopathology in Alzheimer's disease. Acta Neuropathol 103:26–35.

Berger Z, Roder H, Hanna A, Carlson A, Rangachari V, Yue M, Wszolek Z, Ashe K, Knight J, Dickson D, Andorfer C, Rosenberry TL, Lewis J, Hutton M, Janus C (2007) Accumulation of pathological tau species and memory loss in a conditional model of tauopathy. J Neurosci 27:3650–3662.

Busciglio J, Lorenzo A, Yeh J, Yankner BA (1995) beta-amyloid fibrils induce tau phosphorylation and loss of microtubule binding. Neuron 14:879–888.

Callahan LM, Vaules WA, Coleman PD (2002) Progressive reduction of synaptophysin message in single neurons in Alzheimer disease. J Neuropathol Exp Neurol 61:384–395.

Catania C, Sotiropoulos I, Silva R, Onofri C, Breen KC, Sousa N, Almeida OF (2009) The amyloidogenic potential and behavioral correlates of stress. Mol Psychiatry 14:95–105.

Cereseto M, Reinés A, Ferrero A, Sifonios L, Rubio M, Wikinski S (2006) Chronic treatment with high doses of corticosterone decreases cytoskeletal proteins in the rat hippocampus. Eur J Neurosci 24:3354–3364.

Cerqueira JJ, Mailliet F, Almeida OF, Jay TM, Sousa N (2007) The prefrontal cortex as a key target of the maladaptive response to stress. J Neurosci 27:2781–2787.

Chouliaras L, Rutten BP, Kenis G, Peerbooms O, Visser PJ, Verhey F, van Os J, Steinbusch HW, van den Hove DL (2010) Epigenetic regulation in the pathophysiology of Alzheimer's disease. Prog Neurobiol 90:498–510.

Csernansky JG, Dong H, Fagan AM, Wang L, Xiong C, Holtzman DM, Morris JC (2006) Plasma cortisol and progression of dementia in subjects with Alzheimer-type dementia. Am J Psychiatry 163:2164–2169.

Elgh E, Lindqvist Astot A, Fagerlund M, Eriksson S, Olsson T, Näsman B (2006) Cognitive dysfunction, hippocampal atrophy and glucocorticoid feedback in Alzheimer's disease. Biol Psychiatry 59:155–161.

Ewers M, Buerger K, Teipel SJ, Scheltens P, Schröder J, Zinkowski RP, Bouwman FH, Schönknecht P, Schoonenboom NS, Andreasen N, Wallin A, DeBernardis JF, Kerkman DJ, Heindl B, Blennow K, Hampel H (2007) Multicenter assessment of CSF-phosphorylated tau for the prediction of conversion of MCI. Neurology 69:2205–2212.

Gatz M, Reynolds CA, Fratiglioni L, Johansson B, Mortimer JA, Berg S, Fiske A, Pedersen NL (2006) Role of genes and environments for explaining Alzheimer disease. Arch Gen Psychiatry 63:168–174.

Ghosal K, Vogt DL, Liang M, Shen Y, Lamb BT, Pimplikar SW (2009) Alzheimer's disease-like pathological features in transgenic mice expressing the APP intracellular domain. Proc Natl Acad Sci U S A 106:18367–18372.

Green KN, Billings LM, Roozendaal B, McGaugh JL, LaFerla FM (2006) Glucocorticoids increase amyloid-beta and TAU pathology in a mouse model of Alzheimer's disease. J Neurosci 26:9047–9056.

Grundke-Iqbal I, Iqbal K, Tung YC, Quinlan M, Wisniewski HM, Binder LI (1986) Abnormal phosphorylation of the microtubule-associated protein tau (tau) in Alzheimer cytoskeletal pathology. Proc Natl Acad Sci U S A 83:4913–4917.

Guillozet AL, Weintraub S, Mash DC, Mesulam MM (2003) Neurofibrillary tangles, amyloid, and memory in aging and mild cognitive impairment. Arch Neurol 60:729–736.

Hampel H, Bürger K, Pruessner JC, Zinkowski R, DeBernardis J, Kerkman D,

Leinsinger G, Evans AC, Davies P, Möller HJ, Teipel SJ (2005) Correlation of cerebrospinal fluid levels of tau protein phosphorylated at threonine 231 with rates of hippocampal atrophy in Alzheimer disease. Arch Neurol 62:770–773.

Harper JD, Wong SS, Lieber CM, Lansbury PT (1997) Observation of metastable Abeta amyloid protofibrils by atomic force microscopy. Chem Biol 4:119–125.

Hartmann A, Veldhuis JD, Deuschle M, Standhardt H, Heuser I (1997) Twenty-four hour cortisol release profiles in patients with Alzheimer's and Parkinson's disease compared withnormal controls: ultradian secretory pulsatility and diurnal variation. Neurobiol Aging 18:285–289.

Heneka MT, Nadrigny F, Regen T, Martinez-Hernandez A, Dumitrescu-Ozimek L, Terwel D, Jardanhazi-Kurutz D, Walter J, Kirchhoff F, Hanisch UK, Kummer MP (2010) Locus ceruleus controls Alzheimer's disease pathology by modulating microglial functions through norepinephrine. Proc Natl Acad Sci U S A 107:6058–6063.

Hoover BR, Reed MN, Su J, Penrod RD, Kotilinek LA, Grant MK, Pitstick R, Carlson GA, Lanier LM, Yuan LL, Ashe KH, Liao D (2010) Tau mislocalization to dendritic spines mediates synaptic dysfunction independently of neurodegeneration. Neuron 68:1067–1081.

Ittner LM, Ke YD, Delerue F, Bi M, Gladbach A, van Eersel J, Wölfing H, Chieng BC, Christie MJ, Napier IA, Eckert A, Staufenbiel M, Hardeman E, Götz J (2010) Dendritic function of tau mediates amyloid-beta toxicity in Alzheimer's disease mouse models. Cell 142:387–397.

Jeong YH, Park CH, Yoo J, Shin KY, Ahn SM, Kim HS, Lee SH, Emson PC, Suh YH (2006) Chronic stress accelerates learning and memory impairments and increases amyloid deposition in APPV717I-CT100 transgenic mice, an Alzheimer's disease model. FASEB J 20:729–731.

Kang JE, Cirrito JR, Dong H, Csernansky JG, Holtzman DM (2007) Acute stress increases interstitial fluid amyloid-beta via corticotropin-releasing factor and neuronal activity. Proc Natl Acad Sci U S A 104:10673–10678.

Kimura T, Ono T, Takamatsu J, Yamamoto H, Ikegami K, Kondo A, Hasegawa M, Ihara Y, Miyamoto E, Miyakawa T (1996) Sequential changes of tau-site-specific phosphorylation during development of paired helical filaments. Dementia 7:177–181.

Kimura T, Yamashita S, Fukuda T, Park JM, Murayama M, Mizoroki T, Yoshiike Y, Sahara N, Takashima A (2007) Hyperphosphorylated TAU in parahippocampal cortex impairs place learning in aged mice expressing wild-type human TAU. EMBO J 26:5143–5152.

Kimura T, Fukuda T, Sahara N, Yamashita S, Murayama M, Mizoroki T, Yoshiike Y, Lee B, Sotiropoulos I, Maeda S, Takashima A (2010) Aggregation of detergent-insoluble tau is involved in neuronal loss but not in synaptic loss. J Biol Chem 285:38692–38699.

Lace G, Savva GM, Forster G, de Silva R, Brayne C, Matthews FE, Barclay JJ, Dakin L, Ince PG, Wharton SB (2009) Hippocampal tau pathology is related to neuroanatomical connections: an ageing population-based study. Brain 132:1324–1334.

Landfield PW, Blalock EM, Chen KC, Porter NM (2007) A new glucocorticoid hypothesis of brain aging: implications for Alzheimer's disease. Curr Alzheimer Res 4:205–212.

Lauckner J, Frey P, Geula C (2003) Comparative distribution of tau phosphorylated at Ser262 in pre-tangles and tangles. Neurobiol Aging 24:767–776.

Lupien SJ, McEwen BS, Gunnar MR, Heim C (2009) Effects of stress throughout the lifespan on the brain, behaviour and cognition. Nat Rev Neurosci 10:434–445.

Maeda S, Sahara N, Saito Y, Murayama S, Ikai A, Takashima A (2006) Increased levels of granular tau oligomers: an early sign of brain aging and Alzheimer's disease. Neurosci Res 54:197–201.

Mazanetz MP, Fischer PM (2007) Untangling tau hyperphosphorylation in drug design for neurodegenerative diseases. Nat Rev Drug Discov 6:464–479.

Miller TP, Taylor J, Rogerson S, Mauricio M, Kennedy Q, Schatzberg A, Tinklenberg J, Yesavage J (1998) Cognitive and noncognitive symptoms in dementia patients: relationship to cortisol and dehydroepiandrosterone. Int Psychogeriatr 10:85–96.

Nisenbaum LK, Zigmond MJ, Sved AF, Abercrombie ED (1991) Prior exposure to chronic stress results in enhanced synthesis and release of hippocampal norepinephrine in response to a novel stressor. J Neurosci 11:1478–1484.

Ownby RL, Crocco E, Acevedo A, John V, Loewenstein D (2006) Depression and risk for Alzheimer disease: systematic review, meta-analysis, and metaregression analysis. Arch Gen Psychiatry 63:530–538.

Rapoport M, Dawson HN, Binder LI, Vitek MP, Ferreira A (2002) Tau is essential to beta amyloid-induced neurotoxicity. Proc Natl Acad Sci U S A 99:6364–6369.

Rissman RA, Lee KF, Vale W, Sawchenko PE (2007) Corticotropin-releasing factor receptors differentially regulate stress-induced tau phosphorylation. J Neurosci 27:6552–6562.

Roberson ED, Scearce-Levie K, Palop JJ, Yan F, Cheng IH, Wu T, Gerstein H, Yu GQ, Mucke L (2007) Reducing endogenous TAU ameliorates amyloid beta-induced deficits in an Alzheimer's disease mouse model. Science 316:750–754.

Schneider A, Biernat J, von Bergen M, Mandelkow E, Mandelkow EM (1999) Phosphorylation that detaches TAU protein from microtubules (Ser262, Ser214) also protects it against aggregation into Alzheimer paired helical filaments. Biochemistry 38:3549–3558.

Schubert MI, Kalisch R, Sotiropoulos I, Catania C, Sousa N, Almeida OF, Auer DP (2008) Effects of altered corticosteroid milieu on rat hippocampal neurochemistry and structure—an in vivo magnetic resonance spectroscopy and imaging study. J Psychiatr Res 42:902–912.

Sengupta A, Kabat J, Novak M, Wu Q, Grundke-Iqbal I, Iqbal K (1998) Phosphorylation of tau at both Thr 231 and Ser 262 is required for maximal inhibition of its binding to microtubules. Arch Biochem Biophys 357:299–309.

Shipton OA, Leitz JR, Dworzak J, Acton CE, Tunbridge EM, Denk F, Dawson HN, Vitek MP, Wade-Martins R, Paulsen O, Vargas-Caballero M (2011) Tau protein is required for amyloid β-induced impairment of hippocampal long-term potentiation. J Neurosci 31:1688–1692.

Sotiropoulos I, Cerqueira JJ, Catania C, Takashima A, Sousa N, Almeida OF (2008a) Stress and glucocorticoid footprints in the brain-The path from depression to Alzheimer's disease. Neurosci Biobehav Rev 32:1161–1173.

Sotiropoulos I, Catania C, Riedemann T, Fry JP, Breen KC, Michaelidis TM, Almeida OF (2008b) Glucocorticoids trigger Alzheimer disease-like pathobiochemistry in neuronal cells expressing human TAU. J Neurochem 107:385–397.

Sousa N, Lukoyanov NV, Madeira MD, Almeida OF, Paula-Barbosa MM (2000) Reorganization of the morphology of hippocampal neurites and synapses after stress-induced damage correlates with behavioral improvement. Neuroscience 97:253–266.

Stein-Behrens B, Mattson MP, Chang I, Yeh M, Sapolsky R (1994) Stress exacerbates neuron loss and cytoskeletal pathology in the hippocampus. J Neurosci 14:5373–5380.

Stéphan A, Phillips AG (2005) A case for a non-transgenic animal model of Alzheimer's disease. Genes Brain Behav 4:157–172.

Sun X, Steffens DC, Au R, Folstein M, Summergrad P, Yee J, Rosenberg I, Mwamburi DM, Qiu WQ (2008) Amyloid-associated depression: a prodromal depression of Alzheimer disease? Arch Gen Psychiatry 65:542–550.

Swanson LW (1999) Brain maps: structure of the rat brain. Amsterdam: Elsevier Science.

Takashima A, Honda T, Yasutake K, Michel G, Murayama O, Murayama M, Ishiguro K, Yamaguchi H (1998) Activation of TAU protein kinase I/glycogen synthase kinase-3beta by amyloid beta peptide (25–35) enhances phosphorylation of TAU in hippocampal neurons. Neurosci Res 31:317–323.

Terry RD, Masliah E, Salmon DP, Butters N, DeTeresa R, Hill R, Hansen LA, Katzman R (1991) Physical basis of cognitive alterations in Alzheimer's disease: synapse loss is the major correlate of cognitive impairment. Ann Neurol 30:572–580.

van der Vlies AE, Verwey NA, Bouwman FH, Blankenstein MA, Klein M, Scheltens P, van der Flier WM (2009) CSF biomarkers in relationship to cognitive profiles in Alzheimer disease. Neurology 72:1056–1061.

Wang JZ, Gong CX, Zaidi T, Grundke-Iqbal I, Iqbal K (1995) Dephosphorylation of Alzheimer paired helical filaments by protein phosphatase-2A and -2B. J Biol Chem 270:4854–4860.

Wang JZ, Grundke-Iqbal I, Iqbal K (2007) Kinases and phosphatases and tau sites involved in Alzheimer neurofibrillary degeneration. Eur J Neurosci 25:59–68.

Weiner MF, Vobach S, Olsson K, Svetlik D, Risser RC (1997) Cortisol secretion and Alzheimer's disease progression. Biol Psychiatry 42:1030–1038.

Wilson RS, Evans DA, Bienias JL, Mendes de Leon CF, Schneider JA, Bennett DA (2003) Proneness to psychological distress is associated with risk of Alzheimer's disease. Neurology 61:1479–1485.

Wilson RS, Schneider JA, Boyle PA, Arnold SE, Tang Y, Bennett DA (2007) Chronic distress and incidence of mild cognitive impairment. Neurology 68:2085–2092.

Neurobiology of Disease 42 (2011) 404–414

Contents lists available at ScienceDirect

Neurobiology of Disease

journal homepage: www.elsevier.com/locate/ynbdi

Differential regional distribution of phosphorylated tau and synapse loss in the nucleus accumbens in tauopathy model mice

Taiki Kambe [a], Yumiko Motoi [a,*], Ran Inoue [b], Nobuhiko Kojima [c], Norihiro Tada [d], Tetsuya Kimura [e], Naruhiko Sahara [e,f], Shunji Yamashita [e], Tatsuya Mizoroki [e], Akihiko Takashima [e], Kohei Shimada [a], Koichi Ishiguro [a], Hiroshi Mizuma [g], Hirotaka Onoe [g], Yoshikuni Mizuno [h], Nobutaka Hattori [a]

[a] Department of Neurology, Juntendo University School of Medicine, Tokyo, Japan
[b] Department of Molecular Neuroscience, Graduate School of Medicine and Pharmaceutical Sciences, University of Toyama, Japan
[c] Department of Neurobiology & Behavior, Gunma University School of Medicine, Japan
[d] Atopy Research Center, Juntendo University Graduate School of Medicine, Japan
[e] Laboratory for Alzheimer's Disease, RIKEN Brain Science Institute, Japan
[f] Department of Neuroscience, University of Florida, USA
[g] Functional Probe Research Laboratory, RIKEN Center for Molecular Imaging Science, Japan
[h] Department of Neurology, Juntendo Koshigaya Hospital, Japan

ARTICLE INFO

Article history:
Received 17 October 2010
Revised 29 January 2011
Accepted 3 February 2011
Available online 13 February 2011

Keywords:
Tauopathy
Synapse
Nucleus accumbens
Phosphorylated tau
Anxiety
Wild-type tau

ABSTRACT

Tauopathies differ in terms of the brain regions that are affected. In Alzheimer's disease, basal forebrain and hippocampus are mainly involved, while frontotemporal lobar degeneration affects the frontal and temporal lobes and subcortical nuclei including striatum. Over 90% of human cases of tauopathies are sporadic, although the majority of established tau-transgenic mice have had mutations. This prompted us to establish transgenic mice expressing wild-type human tau (Tg601). Old (>14 months old) Tg601 mice displayed decreased anxiety in the elevated plus maze test and impaired place learning in the Morris water maze test. Immunoblotting of brain tissue identified that soluble tau multimer was increased with aging even though insoluble tau was not observed. In the striatum of old Tg601, the level of AT8- or AT180-positive tau was decreased compared with that of other regions, while PHF-1-positive tau levels remained equal. Phosphorylated tau-positive axonal dilations were present mainly in layers V and VI of the prefrontal cortex. Loss of synaptic dendritic spine and decreased immunohistochemical level of synaptic markers were observed in the nucleus accumbens. In vivo 2-[^{18}F]fluoro-2-deoxy-D-glucose positron emission tomography analysis also showed decreased activity exclusively in the nucleus accumbens of living Tg601 mice. In Tg601 mice, the axonal transport defect in the prefrontal cortex–nucleus accumbens pathway may lead to decreased anxiety behavior. Differential distribution of hyperphosphorylated tau may cause region-specific neurodegeneration.

Introduction

Tau is an abundant microtubule (MT)-associated protein in the CNS that is implicated in the pathogenesis of neurodegenerative diseases known as tauopathies including Alzheimer's disease (AD) and frontotemporal lobar degeneration (FTLD). FTLD includes frontotemporal dementia with parkinsonism linked to chromosome 17 (FTDP-17), Pick's disease (PiD), argyrophilic grain dementia (AGD), progressive supranuclear palsy (PSP), and corticobasal degeneration (CBD) (Cairns et al., 2007; Lee et al., 2001). AD and FTLD differ in terms of the affected brain regions associated with their symptoms. AD is a dementing illness where degeneration of neurons can occur particularly in the basal forebrain and hippocampus with progressive loss of memory. In contrast, FTLD is characterized by predominant destruction of the frontal and temporal lobes and subcortical nuclei including the striatum and the brain stem, with changes in personal and social behaviors often associated with disinhibition and relatively preserved memory function.

The majority of tauopathy model mice have shown behavioral abnormalities such as motor dysfunction or memory impairment. However, to the best of our knowledge, no such mice associated with frontal lobe dysfunction have been reported. Three groups (Lewis et al., 2000; Probst et al., 2000; Spittaels et al., 1999) reported the production of transgenic (Tg) mice overexpressing wild-type tau or mutated tau; these animals showed motor abnormalities associated with the phosphorylated tau or neurofibrillary tangles in the spinal cord or peripheral nerves. Subsequently, several groups including us have succeeded in the generation of tau transgenic lines that showed impaired learning connected with parahippocampal formation (Ikeda

* Corresponding author at: Department of Neurology, Juntendo University School of Medicine, 2-1-1, Hongo Bunkyo-ku Tokyo 113-8421 Japan. Fax: +81 3 5684 0476.
E-mail address: motoi@juntendo.ac.jp (Y. Motoi).
Available online on ScienceDirect (www.sciencedirect.com).

0969-9961/$ – see front matter © 2011 Elsevier Inc. All rights reserved.
doi:10.1016/j.nbd.2011.02.002

et al., 2005; Kimura et al., 2007; Murakami et al., 2006; Ramsden et al., 2005; Santacruz et al., 2005; Schindowski et al., 2006). Furthermore, two groups reported tau transgenic mice (N279K and K369I mutation) with a lesion in the nigro-striatal pathway manifesting parkinsonism (Dawson et al., 2007; Ittner et al., 2008). However, although the data obtained demonstrated memory impairment in AD or parkinsonism in FTLD, these mice did not recapitulate behavioral abnormalities such as changes in personality, social behavior, or disinhibition with frontotemporal dysfunction seen in human patients with FTLD. Only a few tau Tg mice were reported to have impairments in impulse control or impaired anxiety resembling human FTLD (Lambourne et al., 2007; Schindowski et al., 2006; Tanemura et al., 2002). However, the neural substrates of these behavioral abnormalities are not fully established.

The phosphorylation of tau plays a physiological role in regulating the affinity of tau for MTs (Biernat et al., 1993; Bramblett et al., 1993; Jameson et al., 1980; Lindwall and Cole, 1984). MT-bound tau is promoted by dephosphorylation of tau while detachment of tau is promoted by hyperphosphorylated tau. With its ability to modulate MT dynamics, tau contributes to key structural and regulatory cellular functions, such as maintaining neuronal processes and regulating axonal transport (Ballatore et al., 2007). There are 85 putative phosphorylation sites on the longest human tau isoform (Hanger et al., 2007; Morishima-Kawashima et al., 1995a). Using either direct sequencing methods or indirect methods such as phospho-specific tau antibodies, many phosphorylation sites on insoluble tau from AD brain have been identified (Hanger et al., 2009, 1998, 2007; Morishima-Kawashima et al., 1995a). Fetal tau is highly phosphorylated at ~18 sites (Morishima-Kawashima et al., 1995b) with stoichiometry (Kenessey and Yen, 1993) of phosphorylation similar to that in AD brain (Brion et al., 1993). However, fetal tau is functional and is not polymerized into NFTs, whereas hyperphosphorylated tau from AD brain inhibits MT assembly and polymerizes into NFTs (Alonso et al., 1994, 2006; Iqbal et al., 1986; Yoshida and Ihara, 1993). This raises the possibility that critical phosphorylation sites exist in addition to these fetal tau phosphorylation sites. Direct analysis of tau from PSP brain identified new phosphorylation sites (Wray et al., 2008). Tau phosphorylation might also be critical for the development of FTLD although the precise molecular mechanisms involved in tau-mediated neurodegeneration might not be identical for all tauopathies.

To investigate how tau affects neuronal function in various brain regions, we generated mice expressing wild-type human tau (Tg601) and examined them. We did not use mutated tau as a transgene because the majority of human tauopathies are sporadic and less than 10% of FTLD and tauopathies have tau mutations (Boeve and Hutton, 2008; Stanford et al., 2004). Different from previously generated tau Tg lines, our mice showed decreased anxiety behavior similar to disinhibition in human FTLD; they showed morphological alterations indicative of dysfunction of the prefrontal cortex–nucleus accumbens (Nac) pathway. The pattern of hyperphosphorylated tau level in the striatum including Nac was different from that in other regions.

Materials and methods

Generation of Tg601 mice

An EcoRI–NdeI fragment of human tau cDNA [2N4R; PRK172 (Goedert et al., 1989)] was treated with Klenow fragment and inserted into the Eco RV site of the vector, pNN265 (Kojima et al., 1998). To add the calcium/calmodulin-dependent protein kinase IIα (CAMKIIα) promoter to this construct, tau cDNA fragment with the 59 intron and simian virus 40 poly(A) signal sequences was excised using NotI and inserted into pNN279 as described previously (Fig. 1A) (Kojima et al., 1998). The transgene was excised from the vector and gel-purified. The transgene was microinjected into the pronuclei of fertilized eggs, and then the transgene-injected eggs were transplanted into the oviducts of pseudopregnant mice.

All of the mouse strains were conceived on an identical genetic background, C57BL/6, and all of the mice used in the present study were heterozygous. As a negative control, nontransgenic littermates were used. The offspring were housed in groups of three to five in a controlled environment with a 12 h light/dark cycle (lights on at 7:00 AM), ambient humidity of 50±10%, and a room temperature of 24±1 °C. Food and water were available ad libitum. The transgene-positive lines were established by crossing founders with C57BL/6J mice. The genotypes of Tg mice were determined by PCR of tail DNA using specific

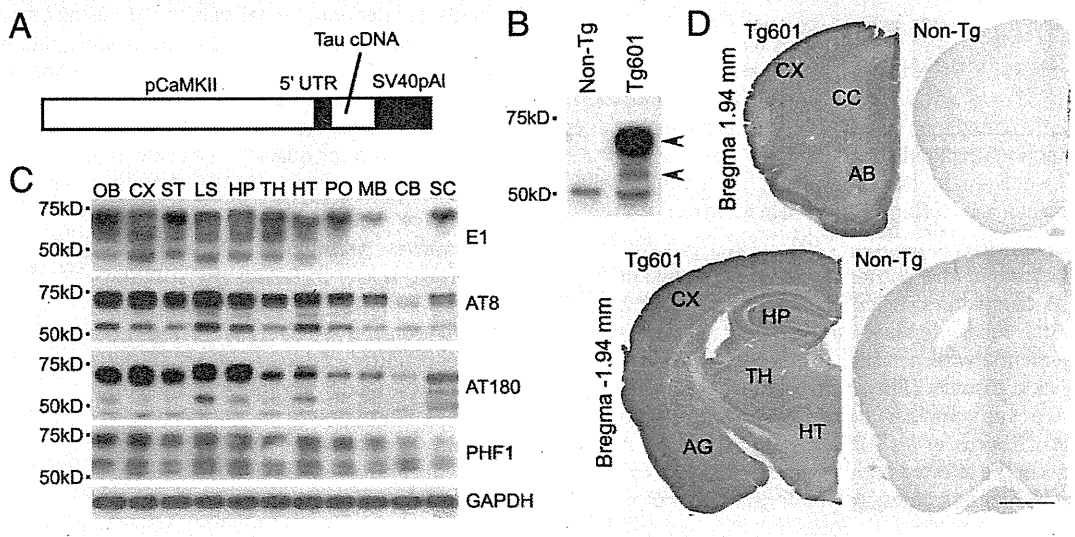

Fig. 1. Characterization of Tg601 mice. A, Transgene construct for Tg601 mouse generation was composed of a promoter region from the Ca^{2+}/calmodulin-dependent protein kinase II gene (pCaMKII), 5′-untranslated region (5′-UTR) derived from pNN265, 3′-untranslated region containing a poly(A) signal sequence (SV40pA1 or SV40pA2), and Tau cDNA. B, Western blotting of extracts of the whole brain derived from wild-type and Tg601 mice with the phosphorylation-independent anti-tau antibody tau5 (which recognizes human tau and murine tau). The expression of transgenic tau is 5.5-fold higher than that of endogenous tau. Arrowheads indicate human tau. C, The pattern of tau expression in different brain regions of 6-month-old female Tg601 mouse was determined by immunoblotting using anti-tau antibodies E1, AT8, AT180, and PHF1. D, Immunohistochemistry of anti-tau antibody E1 (which recognizes human but not murine tau) reveals widespread expression of transgenic tau in 6-month-old female Tg601 mouse. No staining is observed in non-Tg. Scale bars, 1 mm. OB, olfactory bulb; CX, cerebral cortex; CC, corpus callosum; ST, striatum; LS, limbic system; HP, hippocampus; TH, thalamus; HT, hypothalamus; MB, midbrain; PS, pons; CB, cerebellum; SP, spinal cord; AB, nucleus accumbens; AG, amygdala.

primers to amplify the DNA sequence of SV40pA: 5′-TGGAACTGAT-GAATGGGAGCAG-3′ and 5′-AGTGCAGCTTTTTCCTTTGTGG-3′, and of human tau: 5′-CATGGTCAGTAAAAGCAA-3′ and 5′-GGCGGAAGACGGC-GACTT-3′. At 2–18 months of age, female offspring of the Tg601 mice (generations 3–15 obtained by backcrossing with C57BL/6J mice) were subjected to experiments. Experiments were designed so as to minimize the number of animals used and their suffering. All animal experiments were performed in accordance with regulations outlined by Japanese law and National Institutes of Health guidelines, and were approved by the Animal Care and Experimentation Committee of Juntendo University.

Antibodies

The following antibodies were used: human tau-specific E1, which was raised against tau polypeptides corresponding to amino acid residues 19–33; Tau5 (Chemicon, Temecula, CA), which recognizes total phosphorylation-independent human and murine tau; phosphorylation-dependent mouse monoclonal anti-tau AT180 (Innogenetics, Zwijndrecht, Belgium), which recognizes tau phosphorylated at Ser231; AT8 (Innogenetics, Zwijndrecht, Belgium), which recognizes tau phosphorylated at Ser202 and Ser205; PHF-1 (generously provided by Dr. Peter Davies, Albert Einstein College of Medicine, NY), which recognizes tau phosphorylated at Ser396 and Ser404; PSD95 (postsynaptic density-95, BD Biosciences, San Diego, CA), a postsynaptic membrane adherent cytoskeletal protein; Drebrin (Medical and Biological Laboratories, Nagoya, Japan), an actin-binding protein highly enriched in dendritic spines; Neu-N (Chemicon, Temecula, CA), which recognizes neuronal nuclei; polyclonal glial fibrillary acidic protein (GFAP; Nichirei, Tokyo, Japan); and Iba-1 (Wako Chemical, Japan), a microglial marker.

Western blotting

A sarkosyl-insoluble fraction of tau and soluble fraction of tau were isolated from brain tissues as described previously (Sahara et al., 2002). The method for the western blot is detailed in Supplementary materials and methods.

Histology and immunohistochemical procedures

Immunofluorescence

Mice were deeply anesthetized with pentobarbital (50 mg/kg) and then transcardially perfused with 10% formalin. Brains were postfixed in the same fixative for 16 h and then dehydrated by sequential incubation in a series of ethanols and chloroform. The brains were embedded in paraffin and sectioned (6 μm) in the coronal plane. For immunolabeling, sections were permeabilized and blocked for 1 h at room temperature in 5% normal goat serum. This was followed by overnight incubation at 4 °C with the primary antibodies against PSD95 (1:1000) and Drebrin (1:200). After washing, the sections were incubated for 30 min at room temperature in Alexa Fluor 488 (Molecular Probes, Leiden, The Netherlands) secondary antibodies. After washing, the sections were mounted using Vectashield mounting medium (Vector Laboratories, Burlingame, CA). All of the antibody dilutions and the washing steps were performed in phosphate buffer, pH 7.2, containing 0.05% Tween 20. For anti-PSD95 antibody, incubation with 100 μg/mL proteinase K Solution (Wako) for 18 min at 37 °C was performed as pretreatment. A fluorescent microscope (Nikon Eclipse E800) equipped with Axiovision software (Carl Zeiss, Canada) and a fluorescent microscopic system (Biorevo BZ-9000; Keyence, Japan) were used to analyze the sections.

Immunohistochemistry

Mice were not transcardially perfused and brains were fixed in Bouin solution. Six micrometer coronal sections were obtained from each paraffin block. Endogenous peroxidase was quenched by treating the paraffin sections with 0.3% H_2O_2 and nonspecific binding of antibodies was eliminated by applying 5% normal goat serum for 1 h at room temperature. Primary antibody against AT8 (1:400), AT180 (1:400), PHF1 (1:200), GFAP (1:20), or NeuN (1:2000) was applied overnight at 4 °C, followed by secondary antibody of anti-Mouse Immunoglobulins/Biotinylated (1:300, Dako) for 30 min incubation at room temperature. For avidin-biotinylated peroxidase system, we used streptavidin/HRP (1:300, Dako). All of the antibody dilutions and the washing steps were performed in phosphate buffer, pH 7.2, containing 0.05% Tween 20.

Golgi staining

Golgi staining was performed with an FD Rapid GolgiStain Kit (FD Neuro Technologies, MD, USA).

Gallyas silver staining

To detect neurofibrillary tangles (NFTs), Gallyas silver staining was performed (Iqbal et al., 1991).

Techniques of transmission electron microscopy are detailed in supplemental data.

Behavioral testing

Seven tasks were evaluated, using the tests described in detail by Arendash et al. (2004). The methods for the tests are detailed in Supplementary materials and methods.

Positron emission tomography imaging

For intravenous injection of 2-[^{18}F]fluoro-2-deoxy-D-glucose ([^{18}F]FDG), a venous catheter was inserted into the tail vein, and 5 mL of blood was then collected to confirm normal glucose levels before positron emission tomography (PET) scanning. The mouse was set on the apparatus with head-holding to restrict head movements, and was placed on the bed of a small-animal PET scanner, microPET Focus-220 (Siemens Medical System, TN, USA). Prior to the emission scan, the transmission scan was performed for 30 min using a 68Ge–68Ga pin source (18.5 MBq; Siemens Medical Systems) for attenuation correction. [^{18}F]FDG at a dose of 6.7–14.5 MBq/body dissolved in 0.1 mL of physiological saline was automatically injected via the cannula inserted into the tail vein for 10 s using a syringe pump (PHD-2000; Harvard Apparatus Inc., MA, USA), and emission data were then acquired for 60 min using a 3D list-mode method of data acquisition. The images were reconstructed from the emission data at 30 to 60 min after injection of [^{18}F]FDG using a filtered back-projection (FBP) algorithm for quantitative evaluation of [^{18}F]FDG uptake, by a maximum a posteriori (MAP) algorithm for drawing regions of interest (ROIs) on PET images, with attenuation correction, no scatter correction (Mizuma et al., 2010). Quantitative analysis of [^{18}F]FDG uptake was performed using PMOD software (ver. 3.0; PMOD Technologies Ltd., Zurich, Switzerland). Volumetric ROIs were manually placed on several brain regions according to the fused PET/MR T1-weighted images (Supplemental Fig. 1). The index of [^{18}F]FDG uptake ratio normalized in brain tissues is shown as standardized uptake value (SUV): SUV = tissue radioactivity concentration (MBq/cc)/injected radioactivity (MBq) × body weight (g). For comparison of regional distribution patterns among the groups, the delineated ROI data were acquired from the images and normalized using the following equation: Normalized ratio = regional SUV/whole brain SUV. Statistical analysis was performed using the statistical analysis of parametric mapping (SPM99) software. For SPM analysis, all images were coregistered, and signals from outside of the brain area were removed. In addition, all images were smoothed with a 3 mm isotropic Gaussian kernel. For the group analysis (Tg601 minus non-Tg in old or adult period), 2 different statistical criteria showed $P<0.01$ ($T>3.00$, corrected).

Statistics

Statistical analyses were performed with JMP 7 software (JMP 7, SAS Institute, Cary, North Carolina). Differences between means were assessed by Student's t-test and differences among means by two-way repeated measures ANOVA.

Results

Tg601 mice exhibit hyperphosphorylated tau but no NFTs nor neuronal loss

An 8.5 kb portion of the CAMK-II promoter containing upstream control regions and the transcriptional initiation site drives expression postnatally in forebrain neurons (Fig. 1A, Kojima et al., 1998). In forebrain samples from Tg601, equal amounts of endogenous mouse tau were recovered in extracts collected in the TBS-soluble fractions (Fig. 1B). The highest levels of exogenous tau expression were four- to eightfold higher than those of endogenous tau. The level of exogenous total tau expression was very low in brain stem, cerebellum, and spinal cord. Olfactory bulb, frontal cortex, striatum, limbic system, and hippocampus showed higher expression levels than other regions (Fig. 1C). In the forebrain, the level of phosphorylated tau was low in the striatum compared with that in the olfactory bulb, cerebral cortex, and limbic system. Immunohistochemical analysis using anti-human tau-specific antibody E1 confirmed this regional expression pattern, selectively staining mainly forebrain neurons (Fig. 1D).

In western blots of Tris-buffered saline (TBS)-soluble fractions derived from the brains of Tg601 mice, immunoreactivities for AT8, AT180, PHF1, 12E8, and AT270—antibodies that recognize tau phosphorylated at different serines and threonines—were examined. Immunoreactivities for these antibodies increased with aging, except for AT270 antibody (Figs. 2A, B). Because the Thr181 site is phosphorylated at an early step in the development of NFTs (Augustinack et al., 2002), this site might be already hyperphosphorylated by an adult age. To examine whether or not Tg601 mice form tau aggregates, we purified

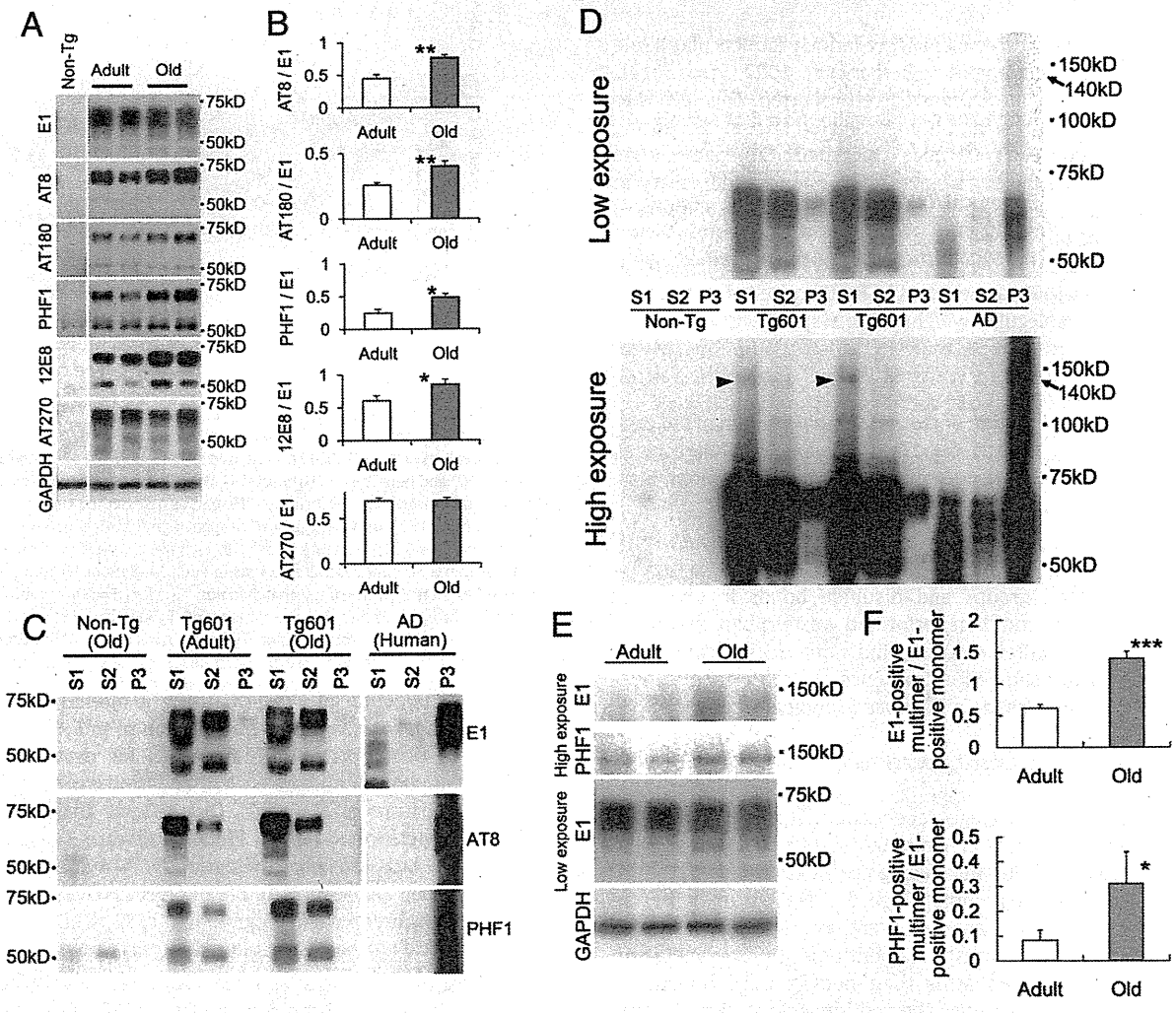

Fig. 2. Western blots of the brain homogenates of 4–8-month-old (adult) and 12–20-month-old (old) Tg601 mice. A. Immunoblotting of TBS-soluble fractions from the brain homogenate. Transgenic tau is identified by human tau-specific E1. Transgenic tau is phosphorylated at epitopes AT8, AT180, PHF1, 12E8, and AT270. B. Quantitative analysis of immunoreactivity for AT8, AT180, PHF1, 12E8, and AT270 in adult (n = 4) and old (n = 6) Tg601 mice. Immunoreactivity for each phosphorylation-dependent antibody was normalized by that of phosphorylation-independent antibody (E1). The results are presented as relative intensity of normalized immunoreactivity in Tg601 mice and expressed as means ± SEM. Immunoreactivity for these phosphorylation-dependent antibodies increased with aging, except for AT270 antibody (*P<0.05, **P<0.01; Student's t-test). C. Western blots of TBS-soluble (S1), sarkosyl-soluble (S2), and sarkosyl-insoluble (P3) fractions from the brains of non-Tg, adult, and old Tg601 mice and a patient with Alzheimer's disease (AD, positive control). Immunoblots were probed with E1, AT8, and PHF1. The brains of AD contained sarkosyl-insoluble tau aggregates, as expected, but the brains of Tg601 mice did not. D. Tau multimer in old Tg601 mice. Tau multimer migrating at ~140 kDa (called tau140) can be seen in old Tg601 but not in age-matched non-Tg mice, when film is exposed for a longer time. E. Immunoblotting of TBS-soluble fractions from the brain homogenate. Tau multimer is identified by human tau-specific E1 and is phosphorylated at epitope PHF1. F. Quantitative analysis of immunoreactivity of tau multimer for E1 and PHF1 in adult (n = 4) and old (n = 6) Tg601 mice. Immunoreactivity for each antibody was normalized by that of monomer for E1 antibody. The results are presented as relative intensity of normalized immunoreactivity in Tg601 mice and expressed as means ± SEM. Immunoreactivity of tau multimer for these antibodies increased with aging (*P<0.05, ***P<0.001; Student's t-test).

insoluble tau with sarkosyl detergent and analyzed sarkosyl-insoluble fractions by western blotting with E1, AT8, and PHF1 antibodies (Fig. 2C). The sarkosyl-insoluble fractions derived from the brains of Tg601 mice did not display positive tau signals, whereas those derived from the brain of a patient with Alzheimer's disease exhibited strong anti-tau immunoreactivity. Taken together, these observations indicate that, in the brains of Tg601 mice, tau becomes hyperphosphorylated with increasing age, but does not form tau aggregates like NFTs. Furthermore, in brain sections from Tg601 mice stained with the Gallyas method, we did not observe any silver-stained neurons, although the brain sections of P301L mutant human tau-expressing mice (JNPL3) (Lewis et al., 2000) exhibited NFT-like Gallyas silver-positive inclusions (Supplemental Figs. 2A–D). Staining of phosphorylated tau was diffusely spread in cytoplasm but not seen as punctuate and peri-nuclear (Supplemental Fig. 2E). No signs of neuronal loss, astrogliosis, or microglial proliferation were observed in the hippocampus, amygdala, nucleus accumbens, and medial prefrontal cortex of Tg601 mice (Supplemental Fig. 3). In summary, our Tg601 mouse model showed progressive hyperphosphorylation of tau but no NFT formation or neuronal loss.

The possibility that oligomeric tau aggregation products play a role in neurodegeneration in tauopathies (Berger et al., 2007; Sahara et al., 2007), like Aβ oligomers, has recently been reported. This led us to explore the formation of similar early aggregated tau species during pathogenic progression in Tg601 mice. Oligomeric tau species were not observed when the film was exposed for the time necessary to detect ~67 kDa tau. However, after prolonged exposure, we observed what appeared to be oligomeric tau species (termed tau "multimer") migrating with apparent molecular weights of ~140 kDa (termed tau140) (Fig. 2D). Tau140 was detected in Tg601 mice but not non-Tg mice. The apparent molecular weight of this species is sufficiently large to suggest that it is a multimeric structure. To further characterize the tau multimer, we used various antibodies. Tau140 was detected with the E1 antibody and the PHF1 antibody (Fig. 2E). In contrast, tau140 was not detected using the AT8 and AT180 antibodies (data not shown), although we cannot exclude the possibility that these negative results are attributable to insufficient sensitivity.

Our results show that the tau multimer described above is detected in the presence of reducing agents. We therefore performed Tg601 brain extractions under conditions that enabled us to capture the state of sulfhydryl groups and disulfide bonds in vivo (see Materials and methods) and then performed western blot analysis of tau multimer species under reducing and nonreducing conditions. However, these studies showed no evidence of additional disulfide-bond-dependent multimers in Tg601 mice (Supplemental Fig. 4B).

Old Tg601 mice display decreased anxiety and impaired place learning

To investigate the effects of age-dependent multimeric tau on brain function, we assessed anxiety in 1-month-old, 6-month-old, and 16-month-old non-Tg and Tg601 mice using the elevated plus maze test (Fig. 3A). At 1 month and 6 months of age, fear feelings of Tg601 and non-Tg mice were not significantly different, as assessed by the time spent in open arms. By contrast, 16-month-old Tg601 mice spent significantly longer in open arms than non-Tg mice littermates ($P=0.0092$). Thus, old Tg601 mice showed impaired anxiety. Y-maze test was performed to evaluate working memory and it displayed decreased spontaneous alternation in old Tg601 mice compared with that in non-Tg mice ($P<0.05$) (Fig. 3B). We also assessed place learning and memory in non-Tg and Tg601 mice using the Morris water maze test. Old Tg601 mice took significantly longer than non-Tg mice to learn the task in the acquisition test ($P=0.0156$) (Fig. 3C). Memory retention (probe) test results for Tg601 mice were also worse than those for non-Tg mice ($P=0.0275$) (Fig. 3D). Adult Tg601 mice did not display a significant difference between these two tests. The performances of Tg601 mice in all other tasks tested were normal. No differences in

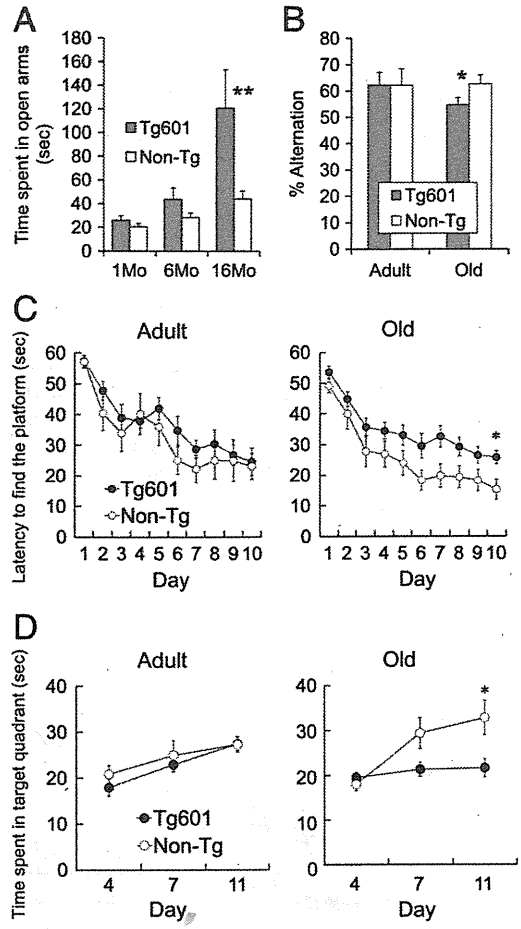

Fig. 3. Tg601 mice show decreased anxiety and impaired place learning. A, The elevated plus maze test was used to assess fear feelings of 1-month-old Tg601 ($n=13$) and non-Tg ($n=16$) mice, 6-month-old Tg601 ($n=18$) and non-Tg ($n=10$) mice, and 16-month-old Tg601 ($n=10$) and non-Tg ($n=10$) mice (A). Fear feelings of 1- and 6-month-old Tg601 and non-Tg mice were not significantly different, as assessed by the time spent in open arms. By contrast, 16-month-old Tg601 mice spent significantly longer in open arms than non-Tg mice (**$P<0.01$; Student's t-test). B, Y-maze test was performed to evaluate working memory. Spontaneous alternations in adult (4–8 months) Tg601 mice ($n=14$) were not different from those of age-matched non-Tg mice ($n=8$). By contrast, in old (12–20 months) mice, spontaneous alternations of Tg601 ($n=18$) were significantly decreased compared with those of non-Tg mice ($n=16$) (*$P<0.05$; Student's t-test). C, The Morris water maze was used to assess place learning and memory. Learning is expressed as latency to find the platform, and memory performance is expressed as time spent in target quadrant during the probe trial. Old (12–20 months) Tg 601 ($n=19$) mice took significantly longer than non-Tg ($n=14$) mice to learn the task ($P=0.0156$, $F=6.5453$) while adult (4–8 months) Tg601 mice ($n=12$) did not show a significant difference compared with the control ($n=12$). D, Memory retention (probe) test result in old Tg601 ($n=17$) mice was also worse than that of non-Tg ($n=12$) mice ($P=0.0275$, $F=5.4304$), while adult (4–8 months) Tg601 mice ($n=12$) did not show a significant difference compared with the control ($n=12$). Results are expressed as means ± SEM. The Morris water maze data were analyzed using two-way ANOVA.

motor function and activity were observed between Tg601 mice and non-Tg mice at 16 months, as tested with the balance beam, string agility, and open field (Supplemental Figs. 5A–C). Over the 4 days of visible platform recognition testing, no significant genotype effect was evident (Supplemental Fig. 5D). Thus, Tg601 mice had no sensorimotor dysfunction or visual impairment that might significantly compromise performance in the cognitive-based tasks.

Tg601 mice display axonal dilatations mainly in cortical layers V and VI of the prefrontal cortex with aging

Immunohistochemical analysis of phosphorylated tau demonstrated AT8-positive axonal dilatations in deep cortical layers V and VI

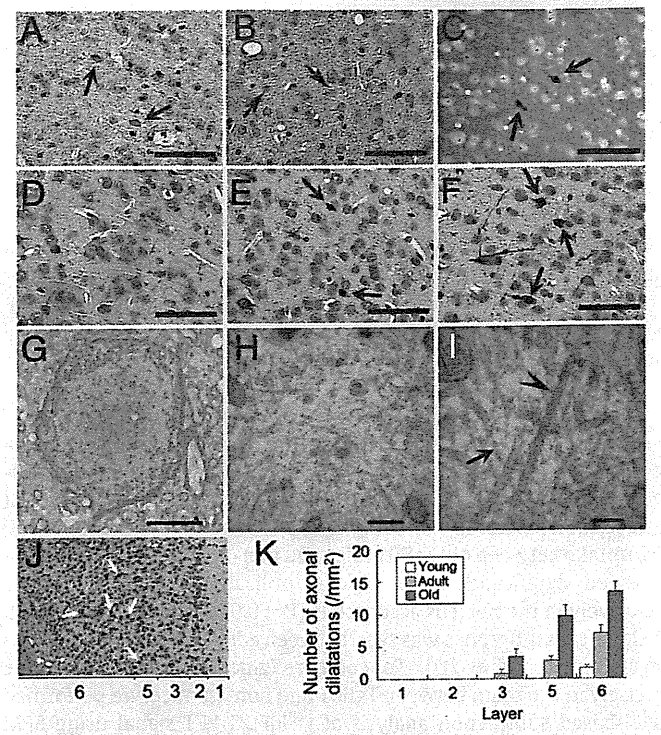

Fig. 4. Immunohistochemical stainings and electron micrographs of axonal dilatations in the prefrontal cortex. A-C. The prefrontal cortex of old Tg601 was stained with AT8 (A) and PHF-1 (B) antibodies and Bielshowsky's silver staining (C). D–F. Anti-phosphorylated neurofilament antibody, SMI-32 antibody immunostained axonal dilatations in the prefrontal cortex of young (2 months), adult (8 months), and old (16 months) Tg601 mice. They increased in number with aging. G–I. Ultrastructure of dilated axons in the prefrontal cortex of Tg601 mice. Dilated axon is distended by the accumulation of neurofilaments, microtubules, mitochondria, and vesicles. Higher magnification of dilated axon showing neurofilaments (arrowhead) and microtubules (arrow, I). J. Schema represents SMI-32-positive axonal dilatations in each layer of the prefrontal cortex. K. Quantitative comparison of the number of SMI-32-positive axonal dilatations among cortical layers in the prefrontal cortex. Young Tg601 (2 months old, n = 3), adult (8 months old, n = 3), and old (16 months old, n = 3) mice were used. Black and white arrows indicate axonal dilatations. Scale bars: 50 μm (A–F); 4 μm (G); 400 nm (H); 100 nm (I).

in the prefrontal cortex of aged Tg601 (Fig. 4A) but not control mice (Supplemental Fig. 6A). A proportion of these structures were PHF-1-positive (Fig. 4B). They were also present in the sensorimotor cortex but were observed in neither the entorhinal cortex nor the piriform cortex. These axonal dilatations were also stained with Bielschowsky's silver impregnation (Fig. 4C) and with SMI-32 antibody (Fig. 4F) and they were also present in the orbitofrontal cortex (Supplemental Figs. 6B–D). They were already observed at 2 months and the number of these structures increased with aging (Figs. 4D–F, K) in Tg601 but not in age-matched non-Tg mice (Supplemental Fig. 6). Ultrastructural examination was performed on the prefrontal cortex of Tg601 mice at the age of 18 months. TEM confirmed that the dilated axons contained neurofilaments, microtubules, and mitochondria (Figs. 4G–I). To examine the distribution of axonal dilatations in cortical layers of the prefrontal cortex, we counted them in five 6-μm SMI-32 antibody-stained sections spaced at 12 μm. The quantitative analysis demonstrated that axonal dilatations were mainly present in layers V and VI in the prefrontal cortex of old Tg601 (Fig. 4K).

Tg601 mice display different regional distribution of PHF1-site phosphorylated and AT8-positive tau

To examine the relationship between tau phosphorylation and decreased anxiety, we performed immunohistochemical and biochemical analyses using the phosphorylation-dependent tau antibodies. AT8 antibody strongly immunostained the cerebral cortex and hippocampus, and moderately stained the cerebellum and brain stem, but only weakly stained the striatum in young Tg601 (Fig. 5A, Supplemental Fig. 7). PHF1 antibody also strongly immunostained the cerebral cortex and hippocampus, but only weakly stained the striatum in young Tg601 (Fig. 5B). In old Tg601, the distribution pattern of AT8-positive tau did not change whereas PHF1-immunoreactivity became strong in the striatum (Figs. 5 C, D). In old non-Tg mice, AT8 antibody showed only faint staining at the edge of the cerebral cortex and PHF1 antibody also showed weak staining in the cerebral cortex (Figs. 5 E, F). To compare the level of phosphorylated tau at various epitopes, we performed western blotting using TBS-soluble fractions derived from the different brain regions including

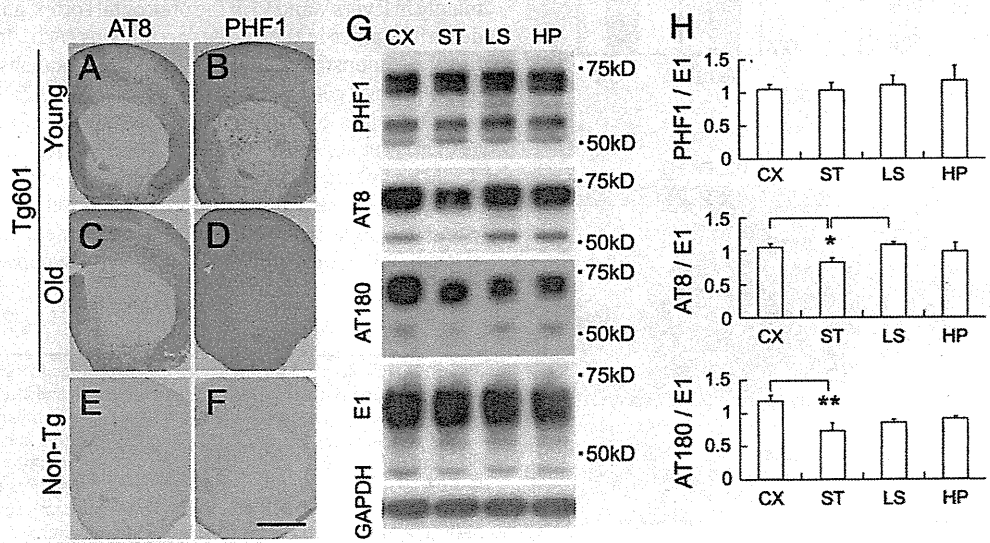

Fig. 5. Regional distribution of phosphorylated tau in Tg601 mouse brains. A–F. Coronal brain sections immunostained with PHF-1 and AT8 antibodies of young (2-month-old) and old (16-month-old) Tg601 mice, and old (16-month-old) non-Tg mice. In young Tg601 mice, both PHF-1 and AT8 antibodies stained the cerebral cortex but not striatum (A, B). Nucleus accumbens is at the ventral side of the anterior commissure, which was strongly stained with PHF-1 and AT8 antibodies. In old Tg601 mice, PHF-1 antibody stained the striatum and cerebral cortex while the staining pattern of AT8 antibody did not change (C, D). G. Immunoblotting of TBS-soluble fractions from the brain homogenate of each area in old Tg601 mice. H. Quantitative analysis of immunoreactivity of each area for PHF1, AT8, and AT180 in old Tg601 mice (n = 3). Immunoreactivity for each phosphorylation-dependent antibody was normalized by that of phosphorylation-independent antibody (E1). The results are presented as relative intensity of normalized immunoreactivity and expressed as means ± SEM. Immunoreactivities of the striatum for AT8 and AT180 antibodies were decreased compared with those of other areas, while that for PHF-1 antibody was equal. *$P<0.05$ compared with CX and LS on AT8. **$P<0.01$ compared with CX on AT180; Student's t-test. Scale bar, 1 mm. CX, cerebral cortex; ST, striatum; HP, hippocampus; LS, limbic system.

the cerebral cortex, striatum, hippocampus and limbic system of old Tg601 mice. Immunoreactivities of the striatum for AT8 and AT180 antibodies were decreased compared with those of other areas, while that for PHF1 antibody was not decreased (Figs. 5B, C).

Old Tg601 mice display loss of synapses and dendritic spines in the nucleus accumbens

To explore which brain region with synapse loss was associated with decreased anxiety behavior, immunohistochemical evaluations of PSD95 and Drebrin, post-synapse markers, were performed in the prefrontal cortex, basolateral amygdala, hippocampus, and accumbens shell. In the accumbens shell, immunoreactivities of PSD95 and Drebrin were significantly reduced in Tg601 mice compared with those in non-Tg mice, while in the prefrontal cortex, basolateral amygdala, and hippocampus, there was no difference (Figs. 6A, B). These significant differences were not detected in the adult (2–8 months). To confirm the synapse loss in the accumbens shell, we also performed Golgi staining. In Tg601 mice, the number of dendritic spines was reduced compared with that in non-Tg mice (Figs. 6C, D).

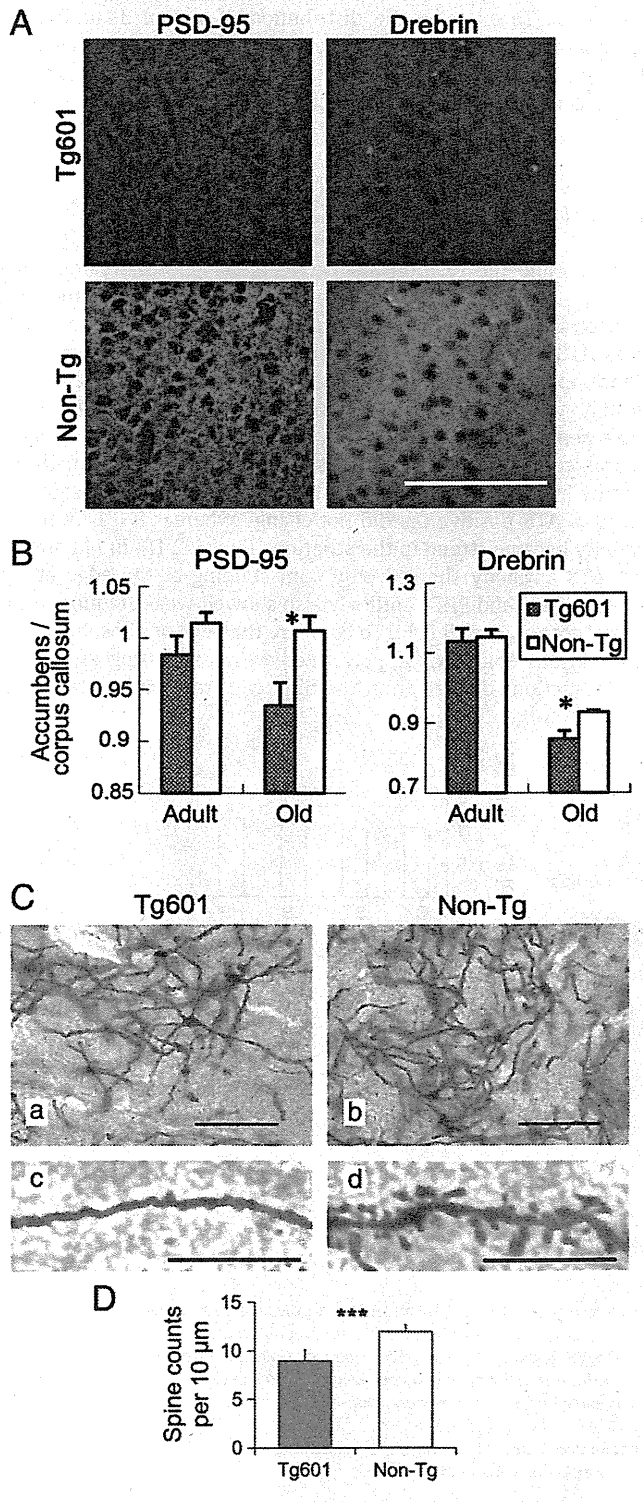

Fig. 6. Synapse loss among accumbens shell neurons in Tg601 mice. A. Immunoreactivities of postsynaptic markers including PSD95 and Drebrin in accumbens shell neurons were reduced in 18-month-old Tg601 mice compared with those in non-Tg mice. B. Quantitative analysis of fluorescence for PSD95 and Drebrin was performed. Fluorescence of each postsynaptic marker in accumbens was normalized by fluorescence in the corpus callosum. Relative fluorescences of PSD95 and Drebrin in old (12–20 months) Tg601 mice (n=3) were significantly lower than those of non-Tg mice (n=3) (*P<0.05 for PSD95, *P<0.05 for Drebrin; Student's t-test). In contrast, these significant differences were not observed between adult (4–8 months) Tg601 (n=3) and non-Tg (n=3) mice. C. Golgi staining showed dendritic spines of accumbens shell neurons of old Tg601 and non-Tg mice. In old Tg601 mice, the number of dendritic spines was reduced compared with that in non-Tg mice. D. Quantification of spine densities in the nucleus accumbens shell of old animals was performed. Data from all dendritic branches were combined. Data represent mean ± S.E. Data were analyzed using Student's t-test and considered significantly different at ***P<0.001. Sixty segments were analyzed from 3 mice for the different groups. Scale bars: 100 µm (A, Ca, and b); 10 µm (Cc–h).

Living old Tg601 mice display decreased glucose metabolism in the nucleus accumbens

To examine which brain regions showed abnormal resting state functional activity in Tg601 mice compared with those of normal non-Tg mice, we performed in vivo PET imaging using 2-[^{18}F]fluoro-2-deoxy-D-glucose ([^{18}F]FDG) and analyzed the regional cerebral glucose metabolism in the living animals. When we compared [^{18}F]FDG uptake between old Tg601 mice and non-Tg mice, old Tg601 mice displayed significantly lower glucose utilization than non-Tg mice exclusively in the nucleus accumbens ($P=0.004$, Fig. 7E). In contrast, no significant difference was seen between adult Tg601 mice and non-Tg littermates (Fig. 7D). To compare glucose metabolism more precisely in the brain between Tg601 and non-Tg mice, we performed voxel-based subtraction analysis of [^{18}F]FDG PET signal using SPM software. The result clearly indicated that a significantly lower [^{18}F]FDG uptake was only observed in the nucleus accumbens of old Tg601 mice but not in the adult Tg601 mice (Fig. 7F). Therefore, we confirmed that Tg601 displayed hypoactivity exclusively in the nucleus accumbens, which is consistent with immunohistochemical findings such as synapse loss.

Discussion

Tg601 mice are unique among tauopathy models in that they show behavioral abnormalities such as decreased anxiety and impaired learning with aging, different regional distribution of PHF-1 site phosphorylated tau from AT8- or AT180-positive tau, axonal dilations mainly in layers V and VI in the prefrontal cortex, and the loss of synaptic dendritic spines in the nucleus accumbens (Acb). In vivo-[^{18}F] FDG-PET further demonstrated decreased glucose metabolism exclusively in the Acb of living Tg601 mice.

In AD, loss of synapses always occurs before death of neurons (Ballatore et al., 2007; Iqbal and Grundke-Iqbal, 2008). In Tg601 mice, the Acb appears to play a key role in decreased anxiety and impaired learning because the synapse loss was observed only in this area. In vivo-[^{18}F] FDG-PET analysis also confirmed this finding because resting state glucose metabolism reflects synapse loss (Rocher et al.,